

RESEARCH MEMORANDUM

INVESTIGATION OF A THREE-STAGE TRANSONIC
RESEARCH AXIAL-FLOW COMPRESSOR

AERODYNAMIC DESIGN AND OVERALL PERFORMANCE

By Melvyn Savage and Loren A. Beatty

Langley Aeronautical Laboratory
Langley Field, Va.

**NATIONAL ADVISORY COMMITTEE
FOR AERONAUTICS**

WASHINGTON

October 27, 1955

Declassified February 8, 1960

NATIONAL ADVISORY COMMITTEE FOR AERONAUTICS

RESEARCH MEMORANDUM

INVESTIGATION OF A THREE-STAGE TRANSONIC

RESEARCH AXIAL-FLOW COMPRESSOR

AERODYNAMIC DESIGN AND OVERALL PERFORMANCE

By Melvyn Savage and Loren A. Beatty

SUMMARY

An investigation of the performance of a three-stage transonic compressor having high stage pressure ratios was conducted as an initial step in an investigation of the problems encountered when high-pressure-ratio transonic stages are grouped together to form a multi-stage compressor. The compressor was designed for an overall stagnation pressure ratio of 2.96 (an average stagnation pressure ratio per stage of 1.44) with a corrected specific weight flow of 29.8 pounds per second per square foot of frontal area at a corrected tip speed of 1,200 ft/sec. Inlet hub-tip radius ratio was 0.50. The overall performance was obtained from tests of the compressor in Freon-12 at corrected speeds from 40 to 100 percent of the Freon equivalent of the design speed in air.

The maximum stagnation pressure ratio obtained at the Freon equivalent design speed was 3.12 at 72.8 lb/sec (corresponding to an air equivalent specific weight flow of 27.7 pounds per second per square foot of frontal area) and an efficiency of 0.82. The peak efficiency at the Freon equivalent design speed was 0.83 and efficiencies as high as 0.82 occurred for pressure ratios ranging from 2.65 to 3.12. The maximum weight flow obtained at design speed was 4 percent less than the Freon equivalent design weight flow. Peak efficiency gradually increased from 0.89 to 0.92 as speed increased from 0.40 to 0.85 of the Freon equivalent design speed. The efficiency remained high over most of the speed range and dropped to just below 0.87 at 0.95 Freon equivalent design speed. The highest overall pressure ratio and weight flow for which an efficiency as high as 0.90 was obtained occurred at 0.92 Freon equivalent design speed (corresponding to approximately 1,100 ft/sec in air) where a pressure ratio of 2.54 (1.364 per stage) was obtained at a weight flow of 71.3 lb/sec. (Air equivalent specific weight flow is 27.1 pounds per second per square foot of frontal area.) At 0.85 Freon equivalent design speed, all three stages appear to be well matched.

The efficiency level (0.90 to 0.92) at this match point is considered to be representative of the performance that should be obtained in an air test at 0.91 air design speed.

An analysis of the effects of using either Freon or air as the test medium for flow through compressor blade rows is also presented.

INTRODUCTION

For high-speed flight, it is desirable that the gas turbine engine be lightweight and compact. Gas turbines which utilize multistage axial-flow compressors can be made lighter and more compact if the compressor has a high flow handling capacity per square foot of frontal area and is composed of stages having high pressure ratios. Transonic rotors have already been shown to be capable of producing pressure ratios of from 1.30 to 1.65 and specific weight flows of from 30 to 36.5 pounds per second per square foot of frontal area at efficiencies of 0.90 (refs. 1 to 3). The performance of such rotors when combined with stators indicated equally high stage efficiencies (refs. 1 and 4).

If several transonic stages are combined into a multistage unit both flow handling capacity and the pressure ratio per stage can be made considerably higher than could be accomplished with subsonic blading. To indicate, however, that efficient transonic rotor and stage performance can be realized in a multistage compressor when several such stages are grouped together, multistage transonic compressors must be designed, built, and tested. Such tests will indicate whether there are adverse effects in grouping transonic stages. For example, they will indicate whether the velocity profiles which develop after several transonic blade rows may adversely affect the compressor performance. They will also indicate whether part-speed performance characteristics of transonic multistage compressors are satisfactory.

To investigate the effects of multistaging several highly loaded transonic stages, an experimental axial-flow compressor having three high-pressure-ratio transonic stages was designed, constructed, and tested at the NACA-Langley Laboratory. The design overall total pressure ratio was 2.96 which corresponded to an average stage pressure ratio of approximately 1.44. The design specific weight flow was 29.8 pounds per second per square foot of frontal area. The original aerodynamic design for this compressor was completed in November 1951. In the interim two other transonic multistage compressors have been designed and tested (refs. 5 and 6). Both showed excellent performance characteristics. The major differences between the compressor herein reported and the first three stages of the transonic multistage compressors of references 5 and 6 are that in this compressor (1) the

solidities are considerably lower; (2) the blade shapes are quite different; (3) all blade selections are based on low-speed cascade data; and (4) the average design stage pressure ratio is about the same as that of reference 5 though accomplished at a higher tip speed and is greater than that of reference 6.

This report presents the design procedure, velocity diagrams, and blading. The overall performance obtained for speeds ranging from 40 to 100 percent of design in Freon is presented. An analysis of the effects of using either Freon or air as the test medium for flow through compressor blade rows is also presented.

SYMBOLS

A	flow area, sq ft
c	blade chord, ft
c_p	specific heat at constant pressure, ft lb/lb/°F
D	D-factor, $1 - \frac{V_e}{V_i} + \frac{\Delta V_T}{2\sigma V_i}$, where velocities are relative to the blade element under consideration
K	boundary-layer blockage factor
M	Mach number
N	corrected rotational speed (the ratio of actual rotational speed to $\sqrt{\theta_T}$), rpm
n	polytropic exponent
P	stagnation pressure, lb/sq ft
p	static pressure, lb/sq ft
Δp	static pressure rise across a blade row, $p_e - p_i$, lb/sq ft
q_i	inlet dynamic pressure, $\frac{\gamma}{2} p_i M_i^2$, lb/sq ft
R	rotor
r	radius, ft
S	stator

SWF	specific weight flow, weight flow per square foot of frontal area, lb/sec/sq ft
s	entropy, ft-lb/lb/°F
T	stagnation temperature, °R
t	static temperature, °R
U	rotational speed, ft/sec
V	velocity, ft/sec
W	weight flow, lb/sec
α	angle of attack, deg
$\Delta\alpha$	difference between actual angle of attack and low-speed cascade design angle of attack, $\alpha - \alpha_{d,c}$, deg
$\Delta\alpha'$	difference between equivalent angle of attack and low-speed cascade design angle of attack, $\alpha' - \alpha'_{d,c}$, deg
β	inlet angle, air direction at inlet to blade row, measured from axial direction, deg
γ	ratio of specific heats
δ	ratio of stagnation pressure to standard sea-level pressure
η	adiabatic efficiency
θ	flow turning angle across blade row, deg
θ_T	ratio of total temperature to standard sea-level temperature
$\Delta\theta'$	difference between equivalent turning angle actually used at design point and the design equivalent value required to fit the design equivalent velocity diagrams, $\theta'_{act} - \theta'$
ρ	density, slugs/cu ft
σ	solidity, ratio of blade chord to blade spacing

Subscripts:

A	air value
a	axial
act	actual equivalent condition used at design point
av	average
B	arbitrary radial station
C	arbitrary radial station
c	low-speed cascade
cr	condition where flow is sonic
d	design
E	Freon equivalent conditions which result for same inlet Mach numbers and inlet angles entering rotor 1 as air design values
e	exit
F	Freon value
h	hub
i	inlet
ideal	ideal
m	mean radius
R	relative to rotor
S	relative to stator
T	tangential
t	tip

Superscripts:

'	equivalent condition, used with flow angles when three-dimensional velocity diagram is converted to an equivalent diagram for blade-selection purposes
---	--

COMPRESSOR DESIGN CONDITIONS AND PROCEDURE

Overall Design Parameters

The three-stage transonic research compressor was designed to be tested in an existing single-stage test stand with a minimum of modification to the test facility. The only effect this had on the design was to fix the compressor tip diameter at 16 inches and the discharge hub-tip radius ratio at 0.75. The following is a summary of the compressor overall design parameters:

- (1) Overall total pressure ratio ≈ 3.0 (average stage pressure ratio ≈ 1.44)
- (2) Equivalent specific weight flow ≈ 30 lb/sec/sq ft frontal area (inlet axial Mach number = 0.555)
- (3) Tip speed = 1,200 ft/sec
- (4) Inlet hub-tip ratio = 0.50
- (5) Exit hub-tip ratio = 0.75
- (6) Constant tip diameter = 16 inches
- (7) Ratio of discharge axial velocity to inlet axial velocity ≈ 0.75

No inlet guide vanes were used in the compressor design.

Tip speed. - Stage pressure ratios can be increased for the same loading limit, that is $\frac{\Delta p}{(P - p)_i}$ or D-factor, by increasing the design rotational speed providing stage efficiency remains the same (ref. 7). For typical transonic inlet rotors without inlet guide vanes the prime factor limiting rotational speed is the level of tip region relative Mach number considered to be acceptable for efficient operation. At the time this compressor was designed and actually even now there is no clearly defined tip limiting Mach number level. In fact, it is felt that Mach number limit is very much determined by blade surface curvature and static pressure rise. A tip relative inlet Mach number of 1.24 was arbitrarily selected for the first rotor. This Mach number combined with a tip speed of 1,200 ft/sec resulted in a design specific weight flow of 29.8 pounds per second per square foot of frontal area. It was hoped that the amount of surface pressure recovery (expressed as the ratio of the overall static pressure rise to the difference between inlet relative stagnation and static pressure) and the shock strength which occurs at an inlet Mach number of 1.24 could be kept low enough

to ensure efficient performance. A moderately large annulus contraction across the first rotor was used to reduce the pressure recovery. To reduce surface Mach numbers and thereby reduce shock strength, thin blade sections with a mean-line shape which tends to reduce the surface curvature in the forward portion of the blade were used for the tip region. If the performance does tend to fall off at this rather high Mach number level, some tip speed lower than the design value of 1,200 ft/sec will be a more desirable operating point.

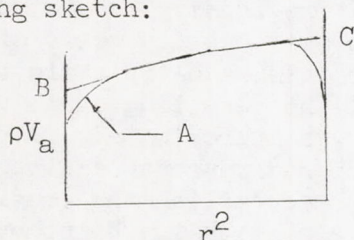
Overall pressure ratio.- The overall total pressure ratio was determined from preliminary hub section calculations in which an arbitrary loading limit of a maximum hub turning angle of between 30° and 31° (based on the mean axial velocity across the hub section) was assumed. For these calculations constant power input radially was assumed as well as a polytropic stage efficiency of 0.90. This hub turning-angle limit provided high pressure ratios while still utilizing blade sections which were within the high-performance range as indicated in the low-speed cascade data of reference 8. As yet, no truly effective loading limit has been obtained which can be used as an absolute loading limit criterion except for blade rows which are similar in pressure rise, solidity, blade shape, thickness, and inlet Mach number to those which have already been tested. Care must be taken to ensure that no $\frac{\Delta p}{(P - p)_i}$ loading limit or D-factor limit is used for conditions too dissimilar from the data which established the limit. Such parameters are only approximate means of estimating the limiting values of surface pressure recoveries which result from complex boundary-layer shock interaction phenomena further complicated by the effects of centrifugal force on blade boundary layer as well as tip clearance effects. The ability to lump these effects into simple overall parameters should therefore not be considered to extend beyond the types of conditions used to establish the limits.

Axial velocity variation.- As stated previously, it was necessary for testing convenience to provide for an exit hub-tip ratio of 0.75. For the design overall pressure ratio, an inlet hub-tip ratio of 0.50, and a constant tip diameter of 16 inches, the resulting axial velocity ratio from compressor discharge to inlet was approximately 0.75. This amount of diffusion in the compressor appeared reasonable since for high-flow machines one problem is where to accomplish the considerable amount of diffusion necessary to obtain velocities in the combustion chamber which are low enough to ensure high combustor efficiencies. By having much of the diffusion take place in the compressor, the length of the diffuser between compressor and combustor can be reduced. Such diffusion in the compressor, however, results in increased pressure recoveries for the various blade rows and hence the blade rows will be operating closer to their aerodynamic loading limits.

Since the maximum inlet relative Mach numbers for this design decreased from the first rotor to the last, the maximum reduction in annulus area occurred across the first rotor in order to reduce surface pressure recovery where it could be most severe.

The hub-tip ratios used in the blade row by blade row computations were obtained from an assumed smooth hub contour from inlet to discharge and from an approximation of the axial projections of the blade rows. Provision was made for approximately a 1.1 inch space between rows for interstage instrumentation. These hub-tip ratios are indicated in table I. The inlet hub-tip ratio for any blade row was taken at the blade leading edge and the exit hub-tip ratio was taken at the blade trailing edge; hence the differences between exit radii from one row and inlet radii for the succeeding row.

Efficiency and boundary-layer blockage factor.- The design of a compressor stage requires that some estimate of stage efficiency and boundary-layer development be made. To attempt an estimation of what the radial distribution of losses will be is not presently feasible unless there are data available for a stage or rotor which is quite similar to that being designed. One method of resolving this problem is to assume an efficiency based on past experience for the free-stream region of the flow in the annulus. This region encompasses most of the blade and is the region for which velocity diagrams are computed and blade sections are selected. The polytropic efficiency assumed for this design was 0.90 for each stage. The small boundary-layer region at the end walls can be accounted for by using past experience to estimate the amount of blockage this boundary layer will produce and then to provide for this blockage by suitably increasing the area. The blockage can be expressed in terms of a blockage factor K which is the ratio of the actual weight flow to the ideal weight flow, W_{ideal} , that would have occurred if there were no reduction in velocity near the casings due to casing boundary layers. An example of K is presented in the following sketch:



$$K = \frac{W}{W_{ideal}} = \frac{\text{Area under curve A}}{\text{Area under curve BC}}$$

Hence, values of K can be readily obtained from test data. A more detailed discussion of blockage factor is presented in reference 9.

A complete discussion of the methods used in the design of the compressor reported herein and the boundary-layer allowances that result

is presented in appendix A. The coordinates for the inner contour that were selected, the assumed K values, and the effective K values that resulted because of the approximation used to satisfy continuity are tabulated in table II. As may be seen, effective K does not gradually decrease from blade row to blade row. Since at the time this compressor was designed little information was available regarding the correct values of K to use, it was not considered necessary to redesign the compressor to provide a gradual smooth decrease in effective K from inlet to discharge. Since the third stage, which has K values greater than 1.0, was considered to have sufficient range to cope with the Mach numbers and angles of attack which would result for a nominal amount of boundary-layer growth at the design point, a recalculation and resetting of this stage for a K of less than 1.0 was considered to be unnecessary. A schematic drawing of the stage transonic compressor is presented in figure 1.

Since the design of this compressor, several transonic rotors and stages have been tested and values for blockage factor and efficiency have been obtained. It has been shown that for stage efficiencies of 0.90 blockage factors of from 0.95 to 0.96 were measured downstream of the transonic rotors (refs. 1 and 4). It was further indicated in reference 1 that downstream of the stator the blockage factors were from 0.94 to 0.95. These values give an indication of blockage factor level that should be used behind the first stage of a multistage transonic compressor. The problem of what values of blockage factor to use for succeeding stages still exists.

A variety of assumptions regarding blockage factor have been made in several successful multistage compressors. For example, no boundary-layer blockage factor was applied in the design of the 10-stage subsonic compressor of reference 10. The eight-stage compressor having two transonic stages (ref. 6) has a blockage factor which decreases steadily from 0.99 in the first stage to 0.77 by the eighth stage. The five-stage transonic compressor (ref. 5) has an assumed blockage factor of 0.95 after the first stage which gradually decreases to 0.90 at the exit of the fifth stage. For the 10-stage compressor at design speed measured weight flow was some 2.7 percent below design; for the eight-stage compressor design weight flow was obtained but not quite design pressure ratio; and for the 5-stage compressor the measured weight flow obtained was about 3.2 percent greater than design.

It should be realized that with the data available it is quite impossible to ascertain how much influence the assumed blockage had on design control, that is, obtaining design conditions. However, it appears that even for rather large variations in assumed blockage the compressor tends to come fairly close to its design weight flow at design speed and pressure ratio providing the rest of the design procedure is reasonable and no obvious loading limits are exceeded. These statements are actually pointing out the fact that if the contraction

through the compressor is somewhat in error it takes only small changes in weight flow to provide reasonable stage matching. Nevertheless, if it can be presumed that turning angles and efficiencies can be estimated with reasonable accuracy, to provide good stage matching at design conditions an accurate method of estimating blockage must be obtained. Analysis of weight-flow distributions behind various stages in several compressors should provide information for estimating such blockage factors.

Velocity Diagram Calculation Procedure

All blade row calculations were made assuming that the flow across each row occurred along conical surfaces generated by maintaining the ratio of radial distance between streamlines to radial passage height constant at the inlet and exit of the row. Hence, each conical surface is defined by

$$\frac{r - r_h}{r_t - r_h} = \text{Constant}$$

As stated previously, the loading limitation used in this compressor design was to keep maximum turning angles, based on mean axial velocity conditions along each conical surface, at approximately 30° to 31° . The determination of the pressure ratio which corresponded to this hub turning angle limitation was a trial and error solution in which the selection of design pressure ratio was altered until the hub turning angle θ_h' was in the 30° to 31° range.

A derivation of the equations used to compute velocity diagrams is presented in Appendix A. The stage-by-stage calculation procedure was as follows:

(1) The relationship between power input and stage stagnation pressure ratio along a streamline is as follows:

$$(U_e V_{T,e} - U_i V_{T,i}) = c_p T_i \left[\left(\frac{P_e}{P_i} \right)^{\frac{n-1}{n}} - 1 \right]$$

The tangential velocity distribution behind each rotor was obtained from this equation used in conjunction with an assumed stage stagnation pressure ratio, the previously assumed value of tip speed ($U_t = 1,200$ ft/sec), a stage polytropic efficiency of 0.90, and the inlet and exit hub-tip

radii. For the first rotor, which has no inlet guide vane, the discharge tangential velocity distribution is free vortex ($V_T \sim \frac{1}{r}$) for the condition of radially constant power input. Application of equation (A9) from the appendix indicated no radial variation in axial velocity at this axial station. Since succeeding stators did not have free-vortex discharge tangential velocity distributions, equation (A9) when applied to rotors 2 and 3 would yield radial variations in rotor discharge axial velocities.

(2) Continuity was satisfied by the method indicated in appendix A and the hub turning angle based on average axial velocity at the hub section was computed. The selection of design stage pressure was adjusted until θ_h' was about 30° to 31° .

(3) To calculate the inlet conditions for the succeeding blade row, constant moment of momentum was assumed across the 1.1 inch gap between blade rows. Therefore, inlet conditions for each succeeding row were obtained by maintaining $V_T r = \text{Constant}$ from the trailing edge of the previous row to the leading edge of the row under consideration. Equation (A9) in conjunction with the satisfaction of continuity was then used to compute the inlet axial velocity distribution. The inlet axial velocity was constant from hub to tip for the first rotor and stator only.

(4) The calculation of conditions downstream of the stator required the assumption of a stator loading limit as well as a selection of the radial variation in exit tangential velocity distribution. Moderately high stator turning angles were necessary to provide high subsonic Mach numbers relative to the succeeding rotor in order to permit the succeeding stage to produce a high pressure ratio. High turning was also necessary to make the inlet angle at the hub section of the succeeding rotor high enough to avoid any possibility of rotor hub choking. As an arbitrary loading limit, stator maximum turning angles were held to from 29° to 32° . Since it was desirable to reduce the tip relative inlet Mach number of rotors 2 and 3 below the rather high value of 1.24 in the first rotor, a solid-body type discharge tangential velocity distribution was used in all stators ($V_T \sim r$). For this type of distribution the maximum turning angles occurred at stator hub sections. The hub exit tangential velocity to accomplish θ_h' values of from 29° to 32° was assumed. The $V_T \sim r$ relationship was applied to obtain the V_T distribution. Just as for rotor calculations equation (A9) and the continuity equation were used to determine the V_a distribution. Several calculations were required to determine the hub V_T selection which would produce θ_h' of the order of from 29° to 32° . The inlet conditions for the succeeding rotor were obtained by applying constant moment of momentum as indicated

in step 2 of the calculation procedure. The calculations of all succeeding stators and rotors were conducted by the same methods as are herein presented.

It should be pointed out that the selection of a maximum stator turning angle of from 29° to 32° was felt to be somewhat conservative but at the time it was not considered advisable to jeopardize the performance of the transonic multistage compressor by using subsonic stators which had considerably higher turning angles than had been currently used. Since then, it has been shown that high turning stators can be used without detrimental effects on the performance of a transonic multistage compressor (ref. 9).

The following stage design total pressure ratios were obtained from these design velocity diagram calculations:

First stage - 1.429
Second stage - 1.458
Third stage - 1.429

A listing of the significant velocity diagram parameters is presented in table I. The maximum rotor inlet Mach numbers were 1.24 in the first rotor, 1.02 in the second, and 0.94 in the third. The maximum value of $\frac{\Delta p}{(P - p)_i}$ was 0.63 for the rotors and occurred at the hub of the first rotor. The maximum value for the stators was 0.55 and occurred at the hub of the third stator. Design velocity diagrams are presented at three radial stations for all three stages (fig. 2).

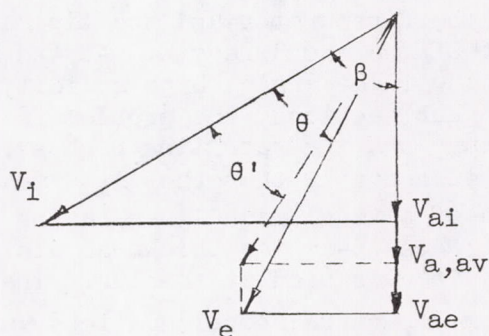
The diffusion factor analysis presented in reference 11 was not available at the time this compressor was designed. The D-factors which resulted from the design velocity diagrams and solidity selections have been computed and are presented in table I. The rotor tip D-factor for the third rotor is higher than the 0.45 limit suggested in reference 11 for subsonic rotors operating below critical speed. Although this limit is exceeded, it is not obvious that the performance of this rotor, which operates at transonic speed with an inlet boundary layer quite different from that of an inlet rotor, will be adversely affected. The maximum stator D-factor occurred at the hub of the third stator and was equal to 0.61. Hence, the stator D-factors do not exceed the limiting values recommended in reference 11.

Equivalent Velocity Diagrams for Blade-Selection Purposes

Since all blade cambers and setting angles were determined from low-speed cascade data, some means of accounting for the variation in

axial velocity which occurred along each conical surface was required. The method used was to calculate so-called equivalent inlet angle and turning angles obtained from the design velocity diagrams by maintaining all tangential components and using the average axial velocity across the blade row along each conical surface. The angles associated with these equivalent constant axial velocity diagrams at each radial station were used in conjunction with low-speed cascade data to determine both the cambers and the blade setting angles with no further recourse to the actual angles associated with the design velocity diagrams.

Since this compressor was designed, a more desirable method of accounting for axial velocity change in a design velocity diagram has been established for the utilization of low-speed cascade data for blade-selection purposes. The suggested method is to maintain the tangential components and to calculate turning angle from the diagram obtained by converting only the discharge velocity to an equivalent discharge velocity based on the mean axial velocity. The resulting equivalent turning angle θ' for the axial velocity increase condition is indicated in the following sketch:



Both of the previously described methods of computing equivalent velocity diagrams for blade-selection purposes represent an attempt to provide either the lower camber necessary for a given turning angle if the axial velocity increased across the blade row in the design diagram (a lower pressure rise condition than occurred in the cascade test) or the higher camber required if the axial velocity decreased in the design diagram. For the axial velocity decrease condition, the method of computing equivalent velocity diagrams where only the discharge velocity is converted to an average velocity results in a lower cambered section operating at the low-speed cascade design angle of attack compared with the other method which results in a higher cambered section operating below its design angle of attack. Both methods provide the same amount of increased or decreased camber as the case may be for a given design velocity diagram since $\frac{d\theta}{d\alpha}$ is generally very close to 1.0 near design angle of attack. The correction method in which only the discharge

velocity is converted to an average velocity, however, is considered to be better because blade setting angle and angle of attack are determined from the actual inlet-flow direction. This fact is important since at transonic relative inlet Mach numbers the angle-of-attack range for efficient performance is less than at subsonic relative inlet Mach numbers. Blade performance may also become quite sensitive to angle of attack at high-flow transonic hub section conditions where blade passage open area is a function of the angle of attack. Hence, it is considered advisable to use a correction system which sets the blade sections relative to an actual inlet velocity direction.

Blade Selection

It has been shown that high blade element efficiency can be obtained at transonic inlet Mach numbers if the maximum blade surface local Mach numbers are kept low. Local blade surface Mach numbers can be reduced by use of thin blades and by a rearward shift in chordwise blade element loading distribution. Hence, the A_2I_8b mean line (ref. 12) was used at the tip section of the first rotor and the tip maximum thickness was chosen to be 6 percent of the chord length. At the hub section because of the combination of low inlet angle, high solidity, and moderately thick blades common to hub sections, the problem is mainly the avoidance of a choked blade passage and the resulting high surface Mach numbers. It has been shown in reference 12 that the A_{10} mean line presents the most open passage area of several mean lines having differing loading distributions when the NACA 65-series thickness distribution is employed. Hence, the A_{10} mean line was used at the hub. The hub maximum blade thickness dictated from structural considerations was selected to be 10 percent. In order to obtain a smooth radial transition in blade profile the A_6I_{4b} mean line was used at the mean radius. The maximum thickness at the mean radius was 8 percent.

Since the stator inlet Mach numbers were generally quite low and the highest inlet Mach numbers occurred at the stator hub where thin sections could be used, it was considered unnecessary to use any mean line other than the conventional subsonic A_{10} for stator blades. The maximum thickness for both first and second stators varied linearly from 6 to 10 percent from hub to tip. Maximum thickness for the third stator varied linearly from 6 to 9.6 from hub to tip.

The NACA 65-series thickness distribution, with a trailing-edge region thickened to a trailing-edge radius equal to 10 percent of the maximum thickness, was used for all blading. Since this compressor was designed, it is felt that a more desirable thickness distribution for transonic performance would have a thinner nose region with its maximum thickness distribution farther back along the blade (ref. 13). By using

a thinner nose region the surface curvature is reduced in a region where it may be highly desirable to keep surface Mach numbers as low as possible.

All blade selections were made using the low-speed cascade data presented in references 8 and 12. From the limited amount of A_6I_{4b} mean-line data that were then available, it was found that sufficient accuracy for design purposes could be obtained for the A_6I_{4b} mean line by arithmetically averaging the corresponding design conditions for the A_{10} and A_2I_{8b} mean-line data. All blading was selected near design angle of attack as determined in the low-speed cascade tests.

It is desirable to limit the number of master blades in order to reduce compressor fabrication time and cost. Hence, whenever it was necessary to use a blade with a higher camber at a slightly lower than design angle of attack for a particular turning angle to eliminate the fabrication of a master, this was done providing such changes were not considered detrimental to the compressor performance. The differences between α' used at design conditions and the α_d as obtained from low-speed cascade tests are tabulated in table III as $\Delta\alpha'$ and are based on equivalent velocity diagrams. The moderately large $\Delta\alpha'$ values for stator 1 resulted from a fabrication error in which the hub and tip blade settings were interchanged. The resulting differences between actual angles of attack and low-speed cascade design angles of attack are indicated as $\Delta\alpha$ in table III.

It was possible to fabricate all three rotors from the same master by cutting off the tip section for the shorter rotor blades. Stators 2 and 3 were fabricated from one master by cutting off the tip (the tip being at the outer casing) for the shorter blades. The deviations between actual equivalent turning angles, which resulted in order to reduce the number of masters, and the required equivalent design turning angles are given in table III in the column marked $\Delta\theta'$. The maximum deviation occurred in the third stator and was 2.2° . Generally, the differences were considerably less than this maximum deviation.

This blading is quite different from the double circular-arc rotor blading used in references 5 and 6. It represents an attempt to use the type of blading at each radial station which appears to be most desirable for the aerodynamic conditions which exist at that radial station. It is difficult to ascertain whether this degree of elaborateness is necessary since excellent multistage performance results were obtained with double circular-arc blading (refs. 5 and 6). It may be that for the levels of Mach number and loading which occurred in the compressors of references 5 and 6 a shift in blade mean line to the types used in this compressor would be a second-order effect. However, it appears reasonable that at some Mach number and loading level a variation in blade shape from hub to tip might improve performance markedly.

Since there is a fairly extensive amount of low-speed data available for blades having A_{10} , A_{2I8b} , or A_{6I4b} mean lines it is felt that the problem of blade selection for compressors having varying blade shapes from hub to tip can be effectively handled.

The tip solidity for rotor 1 was selected as 1.0 because at the time this compressor was designed the effects of lower tip solidities on transonic performance were unknown. Recent high-flow transonic rotor tests (ref. 13) indicated efficient rotor performance with tip solidities as low as 0.75. The hub solidity for rotor 1 was kept as low as possible without requiring too high a camber. It was kept low both to avoid a choked hub section and to improve the blade-row efficiency. An examination of low-speed cascade data indicated that blade element profile drag was almost independent of solidity and hence for the same turning angle or lift, blade row efficiency should increase with decreasing solidity. From such considerations the hub solidity was selected to be 1.25. For this solidity, a $C_{l0} = 1.75$ was required and this camber was well within the efficient operating range as indicated in the low-speed cascade data in reference 8. The rest of the blade solidities were determined from an assumed linear variation in blade chord. To permit this blade to be used for all rotors some variation in solidity was required for rotors 2 and 3. The resulting solidities are indicated in table III.

Stator solidities were kept at least as high as 0.95 and are indicated in table III. It was necessary to use a solidity of 1.385 in the third stator to permit the use of the same stator master as stator 2 while fulfilling the third stator velocity diagram. These solidities were considerably lower than those of the first three stages in the five-stage transonic compressor (ref. 5) where rotor solidities varied from 1.89 to 0.98 and stator solidities varied from 1.89 to 1.20. They were also lower than those of the two transonic stages of the multistage compressor described in reference 6 where rotor solidities varied from 1.86 to 1.19 and stator solidities varied from 1.52 to 0.82.

To facilitate blade fabrication all blade section profiles were applied at the average of the inlet and exit radii for each conical surface. Blade element solidities were calculated using these average radii for each conical surface. A complete summary of the compressor blading is presented in table III.

Blade Fabrication and Clearance

All rotor blades were fabricated of duraluminum and were cut on an airfoil duplicating machine. The resulting unpolished surface consisted of chordwise ridges and grooves. The height from groove to ridge was

0.0019 inch and the distance between ridges was 0.044 inch. The rotor blades were used in the unpolished state. If compressor efficiency were as high as that of conventional compressors with polished blades, this might indicate that surface roughness had no serious effect on compressor performance. A photograph of the three rotor assembly is presented in figure 3. All stator blades were cast of fiberglass and paraplex (a polyester resin) with the final surface cast of Armstrong adhesive. The surface finish was quite smooth and approximated a polished metal surface condition.

Rotor tip and stator hub clearances of 0.030 inch were used as design values. A check of the unit indicated that rotor tip clearances were generally close to design values but that the stator hub clearances were greater and nonuniform. The following are clearances measured for the two blades in each stator row located on either side of one-half of the split stator casing:

Stator	Clearance, inches		Clearance, percent average span	
	Left side	Right side	Left side	Right side
1	0.047	0.062	1.5	2.0
2	.074	.076	3.2	3.3
3	.057	.049	2.8	2.4

The clearances are considered to be typical of each stator row. Rather than rebuild the stator blades to reduce these gaps, the compressor was accepted as is for testing.

FREON TESTING

The Use of Freon as the Test Medium for Flow Through Compressor Cascades

Freon-12 has often been used as the test medium for rotor and stage tests since it has a lower speed of sound than air and permits lower rotational speeds to be used for the same Mach number levels. The method of converting Freon test data to equivalent values in air in order that results can be examined on a numerical basis familiar to compressor designers has been presented in reference 14. The Freon equivalent condition corresponding to any air design condition is the combination of rotational speed and weight flow in Freon which makes the mean radius section rotor relative inlet Mach number and the inlet angle the same as the corresponding air design values.

For the above-mentioned equivalence between air and Freon results to have significance, a streamline similarity between flow in air and Freon must exist as well as a similarity in boundary-layer growth along the blade. Streamline similarity assumes that the ratio of the stream-tube area at any two positions must be the same for both fluids. In reference 15, the variation in $\frac{A_{cr}}{A}$ with Mach number was shown to be nearly the same for air and Freon up to a Mach number of about 1.4. A comparison of isolated airfoil pressure distributions over a wide range of inlet Mach numbers and angles of attack (ref. 15) indicated that at the same inlet Mach numbers and angles of attack excellent agreement resulted between air surface pressure coefficients and air equivalent coefficients computed from the Freon tests using the assumption that streamline similarity occurs. These results, of course, do not state that surface Mach numbers or pressure recoveries are identical for air and Freon tests at the same inlet conditions. In fact, an indication of the differences in pressure coefficients for an isolated airfoil is presented in figure 11 of reference 15 where it is indicated that the Freon pressure recovery is actually greater than that obtained in the air test.

If streamline similarity can be assumed to exist for flow through cascades, then A_i/A_e across a blade row will be independent of the test gas. Based on the previously mentioned isolated airfoil results this assumption should be true as long as the boundary-layer growth along the blade does not differ appreciably from one gas to the other because of a more severe pressure recovery in one of the test gases.

Since A_i/A_e on a one-dimensional basis is equal to $\frac{\cos \beta}{\cos(\beta - \theta)}$, streamline similarity states that for the same inlet conditions the turning angle is independent of the test gas. Since turning angle, losses, and efficiency, however, are functions of pressure recovery, it was considered advisable to compare overall pressure recoveries, expressed as $\Delta p / (P - p)_i$ for the two gases over a range of conditions typical of subsonic and transonic blade rows. The flow processes were all assumed to be isentropic. If turning angles are assumed to be independent of the gas, the magnitude of the differences in pressure recoveries that result will indicate to some extent the validity of this turning angle assumption. Comparative computations were made at the same inlet Mach number and inlet-angle conditions for each gas over relative inlet Mach numbers ranging from 0.4 to 1.2 and air static pressure ratios ranging from 1.1 to 1.6. A detailed description of the calculations is presented in Appendix B. In these computations the flow was considered to be shock free in all cases. The results of this comparison are presented in figure 4 where $\frac{\Delta p}{(P - p)_{i_{air}}} / \frac{\Delta p}{(P - p)_{i_{Freon}}}$ is plotted against air static pressure ratio for varying inlet relative Mach number. The Freon test

conditions invariably had the greater amount of loading. For inlet Mach numbers up to 1.0 the differences in loading for the two gases are not large at moderate to large static pressure ratios (1.3 to 1.5). There is some tendency for the difference in loading to become larger at the lower pressure ratio conditions at $M_1 = 1.0$ where the actual pressure recovery in each gas has decreased. At $M_1 = 1.2$ the Freon loading was significantly greater than that in air at the lower static pressure ratio. At first glance this result indicates that in this range of conditions the use of Freon as test fluid results in a much more severe flow process than occurs in air. However, it should be noted that turning angle will generally decrease if some small amount of separation results because the surface pressure rise exceeds the limit for unseparated flow. Hence, part of this large difference in loading could be eliminated by a reduction in turning angle in the Freon case caused by the increased pressure recovery associated with the same turning angle as in the air case. For example, for a $(P_e/P_i)_{air}$ value of 1.4 and $M_1 = 1.2$ condition it takes only a small decrease in turning angle to greatly decrease the Freon pressure recovery since the discharge Mach number is close to 1.0.

In summation, it has now been shown that there are differences in loading expressed in terms of pressure recoveries for the two gases. The differences are small for Mach numbers up to 1.0 but quite large for higher inlet Mach numbers unless some reduction in turning angle results for the Freon conditions at these higher inlet Mach number conditions. These observations were all based on external flow parameters without recourse to what occurs in the blading. Based on the measured pressure distribution results presented in reference 15 the Freon pressure coefficients and hence surface Mach numbers will be higher than those of the air test at the same inlet conditions. Hence, the above-mentioned loading differences would be amplified somewhat if actual blade-surface pressure recoveries were examined.

Since transonic blade rows will have a normal shock somewhere on the suction surface, it was considered advisable to compare the pressure recovery across normal shocks of varying strength for the two gases. Such a comparison is presented in figure 5 where the ratio of the pressure recoveries is plotted against shock inlet Mach numbers. The Freon conditions again indicated the greater amount of pressure recovery and hence the greater likelihood of flow separation. Of course, there is the question regarding whether the shock inlet Mach number would be the same for a cascade tested in both gases. Based on the previously mentioned isolated airfoil tests it might be greater in Freon but based on the same amount of turning along the blade for a transonic relative inlet Mach number it would be less in Freon.

Hence, from both detailed surface conditions as well as on an overall basis the Freon loading will very likely be greater than would occur in air. If the assumption were made that losses increase with pressure recovery, Freon test results should show greater losses than an air test for the same inlet conditions.

The comparison based on constant turning angle was expanded to compare static-pressure ratios and density ratios in the two gases. The results of these computations are presented in figures 6(a) and 6(b) where ratios of air and Freon static-pressure ratios and static-density ratios are plotted against air static-pressure ratio for various inlet Mach numbers. The variation in the ratio of air to Freon static-pressure ratio is nearly linear with air static-pressure ratio for any particular inlet Mach number. Over the range of conditions examined, the air condition always exhibited a higher static-pressure ratio. It is some 5 percent greater than the Freon value at an air p_e/p_i of 1.4 and $M_i = 1.0$. The combination of higher static-pressure ratios in air coupled with the possibility of lower losses in air associated with the lower pressure recoveries at higher Mach number conditions, indicates that air efficiencies could be greater than those measured in the Freon tests. As a result, Freon efficiencies might well be conservative in their indication of potential air performance.

The density ratio variation is quite small except for conditions much above $M_i = 1.0$. At $M_i = 1.0$ and a static-pressure ratio of 1.4 the Freon density ratio is about 1.5 percent greater than the corresponding air value. Density differences of this order are mainly significant for stage matching considerations.

In summation, the conversion of design conditions for a transonic blade row designed for air operation to equivalent design conditions for Freon at the equivalent condition of mean radius inlet Mach number and inlet angle at least on a two-dimensional basis should result in approximately the same turning angles in Freon as in air and lower pressure ratio and higher density ratio than the air design values. Blade loading should be approximately the same in either test fluid for Mach numbers up to 0.80 with the possibility of considerably greater loadings for higher Mach numbers in Freon tests. Hence, Freon efficiencies for such conditions may actually be conservative when considered to be a measure of the efficiency of the corresponding air test (the air test at the same inlet Mach number and inlet angle). In a comparison of Freon test data with air design values, suitable changes in design pressure and density ratios should be made.

Freon Testing of a Multistage Compressor

Designed for Air Operation

Because of bearing difficulties as well as stress problems associated with the higher speed test conditions, the tests of the compressor reported herein were all made in Freon. This compressor was designed and contoured for air operation. The difference in density ratio across a blade row for air and Freon while not too significant for rotor or stage work is quite significant in multistage compressor work when a compressor designed for one gas is tested in the other. If Freon equivalent speed and weight flow were determined by matching the air values of inlet relative Mach number and inlet angle of the first rotor at the mean radius, the compressor stages would not be matched at this operating point even though they were perfectly matched at the air design point. The accumulative effect of even a few percent difference in density ratio per blade row would result in considerable mismatch at the back end of the compressor.

As an indication of the degree of mismatch that would result, a one-dimensional mean radius calculation for Freon was made through the compressor at the Freon equivalent design speed and weight flow of the first rotor. The assumptions made were that efficiency remained constant at 0.90 per blade row and that the relative flow direction leaving each row was constant and equal to the air design values. Continuity was satisfied on a one-dimensional basis (similar to what was done in the air design, Appendix A) and a blade row by blade row calculation was completed to determine the angles of attack for each blade row. This procedure entails a trial and error solution across each row. The deviations from the air design angles of attack that resulted for this Freon calculation are presented in figure 7. A maximum deviation ($\alpha - \alpha_d$) of 9.3° was found to occur at the last blade row. A similar computation was made in which the axial velocity entering the first rotor was increased to determine how much increase in flow would be required to reduce this rather large maximum deviation. The deviations from design angles of attack for a V_{a_1} of $1.072 (V_{a_1,E})_{\text{Freon}}$ are also presented in figure 7. This increase of 7.2 percent in V_{a_1} has reduced the deviation in the third stator to 1.8° . However, the first stator deviation became -3.3° . This result indicates that the V_{a_1} choice was slightly too large to produce the minimum absolute value of deviation. A lower V_{a_1} would have produced a minimum absolute value of deviation of somewhere between 1.8° and 3.3° . Hence, at Freon equivalent design speed only a fair match of angles of attack can be obtained even at a higher Freon weight flow than the weight flow which corresponds to Freon equivalent conditions for rotor 1. (The 7.2 percent increase in V_{a_1}

corresponds to almost a 5 percent increase in weight flow.) All Mach numbers at this match point are greater than the air design values. The following tabulation presents a comparison between rotor inlet relative Mach numbers for this match point and the air design values.

Rotor	$M_{iR,m}$ for -	
	Air design	Match point
1	1.00	1.03
2	.91	.97
3	.87	.95

From these results it appeared desirable to determine whether a closer matching of angles and Mach numbers could be obtained at some other combination of Freon speed and weight flow. It was reasoned that since the first rotor has the highest Mach numbers and α range is reduced at high Mach numbers, the match condition Freon inlet angles to rotor 1 should be identical with the air design values. This assumption fixes the ratio of speed to inlet axial velocity. It was then necessary to determine the speed and axial velocity level at which a close match of flow angles and Mach numbers would exist in Freon. As a first trial in the determination of a Freon match point the combination of Freon speed and weight flow which provided both the same relative inlet angle and absolute exit angle at the mean radius of rotor 1 as the air design was determined. For this combination of speed and flow, a one-dimensional mean radius calculation was made for the rest of the blade rows. The computation procedure and assumptions were the same as those mentioned in the previous section for a similar type of mean radius calculation. The resulting deviations in angles of attack from the air design values are indicated in figure 8. It is labeled condition 1 and corresponds to a Freon inlet axial velocity and rotational speed of 0.964 of the Freon axial velocity and rotational speed at which Freon relative inlet Mach numbers and inlet angles of rotor 1 are the same as the air design conditions. That is, condition 1 corresponds to 0.964 of the Freon equivalent speed and axial velocity that would result if rotor 1 were treated as a single rotor using the methods of obtaining Freon equivalent conditions previously recommended for single rotors or stages. The deviation in angle of attack reached a maximum of 3.8° at the third stator. By using for condition 2 a Freon axial velocity and rotational speed which was 1 percent lower than condition 1 (that is, 0.955 of the first rotor Freon equivalent speed and V_{a1}) the maximum deviation was reduced to 2.2° (fig. 8). On the basis of the results of these trials it appears that a fairly good match point (maximum deviations of the order of 1° with the first row angle operating exactly at the air design

angles of attack) could be realized at a rotational speed and axial velocity of approximately 94 percent of the corresponding first rotor equivalent Freon conditions. This match condition corresponds to approximately 96 percent of the Freon equivalent design weight flow for rotor 1. The mean radius relative inlet Mach numbers for rotors 1, 2, and 3 at this match condition were 0.95, 0.91, and 0.89, respectively, compared with air design values 1.00, 0.91, and 0.87. Hence, only rotor 1 was operating at a significantly lower Mach number level.

Hence, if the compressor were perfectly matched in air at design speed it should be fairly well matched at axial velocity and speed conditions corresponding to 94 percent of the first rotor equivalent Freon speed and axial velocity conditions. It has therefore been shown that a fairly good match condition can be established for the three-stage compressor when it is tested in Freon even though it was contoured and designed for testing in air. It is therefore concluded that the Freon performance is indicative of the compressor performance that should occur in the air test as long as the previously mentioned differences in match points and overall pressure ratios are considered when the test results are examined.

For multistage compressors which have considerably higher overall pressure ratios and hence more stages than the three-stage compressor reported herein, the use of Freon as the test medium for a compressor designed for air operation is considered to be undesirable. It is doubtful that a close match of air design angles and Mach numbers for all stages could be had in Freon even on a one-dimensional basis. Hence, if Freon must be used as the test medium for such compressors, it is recommended that the compressor be designed for Freon. While a compressor designed for Freon testing could not be used directly in an air application, a comparison of the design conditions and the measured results in Freon would indicate the quality of the design system employed.

COMPRESSOR INSTALLATION, TEST PROGRAM AND PROCEDURE

Test Rig

The compressor installation used in these tests is a closed-circuit rig equipped to use either Freon or air as a testing medium. A schematic diagram of the layout is shown in figure 9. This installation has a 3,000-hp induction motor driven by a variable-frequency power supply. Using the gear ratio of 2.015 to 1, the maximum compressor rotational speed possible was 13,300 rpm. The speed was maintained constant by an electronic control and was measured by an electric chronometric tachometer. The axial locations of the inlet and exit measuring stations are indicated in figure 1. The inlet measuring station is approximately

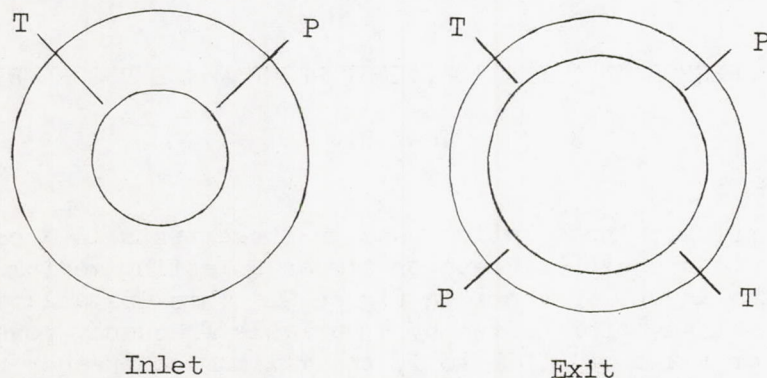
3.25 inches upstream of the first rotor and the exit measuring station is about 3.75 inches downstream of the last stator row.

Instrumentation and Data Reduction

Compressor equivalent weight flow was determined from the calibrated venturi (fig. 9), and measurements of stagnation pressure and temperature made in the settling chamber. Stagnation pressure in the settling chamber was determined from four static taps located there and stagnation temperature was obtained from four shielded thermocouples located in the settling chamber in a vertical line upstream of the compressor inlet.

Inlet instrumentation consisted of: (1) A 10-tube shielded stagnation pressure rake with tube spacing of 0.453 inch between centers (fig. 10, for similar type of rake) and spacing of approximately $7/16$ inch between casings and nearest tube center line, and (2) a stagnation temperature rake (fig. 10) made up of four shielded chromel-alumel thermocouples $1/2$ inch apart on centers and located in the middle region of the annulus.

Exit station instrumentation consisted of: (1) two 10-tube shielded stagnation pressure rakes somewhat similar to the inlet rake but with tube spacing between centers of 0.184 inch (fig. 10) and spacings between casings and nearest bell center line of 0.172 inch and located 180° apart, and (2) two stagnation temperature rakes of the same type as used in the inlet located 180° apart but spaced so that the center of the outermost bell is $5/16$ inch from the outer casing and the center of the innermost bell is $3/16$ inch from the inner casing. The following sketch indicates the circumferential locations of these rakes looking upstream: P corresponds to pressure rake and T to temperature rake.



The differences between the overall downstream pressures obtained by averaging the 10 readings for each of the exit rakes was found to be negligible. Therefore, one of the downstream rakes was removed and overall total pressure ratio was obtained from numerical averages of the

readings obtained from single upstream and downstream rakes. It should further be pointed out that the differences between the 10 stagnation pressure readings at the compressor inlet and the settling chamber stagnation pressures were negligible.

Overall temperature rise was obtained by numerically averaging the 8 temperature rises obtained from the two exit station temperature rakes, which were connected to the four-bell upstream temperature rake to read the temperature differential across the compressor. Efficiency was computed from the following equation using numerical averages for measured pressure and temperature ratios:

$$\eta = \frac{\left[\left(\frac{P_e}{P_i} \right)^{\frac{\gamma-1}{\gamma}} - 1 \right]}{\left[\left(\frac{T_e}{T_i} \right) - 1 \right]}$$

Four outer casing static pressure wall taps, 90° apart, were located behind each blade row. To determine stage tip section static pressure ratios, the inlet static pressure to rotor 1 was computed from the venturi weight flow, the settling chamber stagnation temperature and pressure, and the annulus area at $r_r/t_t = 0.50$.

The accuracy of the measurements is estimated to be within the following limits:

Temperature, °F	±1.0
Pressure, in. hg	±0.03
Weight flow, percent	±1.0
Speed, percent	±0.5

Scope of Tests

The compressor was tested in Freon-12 at corrected speeds of 40, 50, 60, 70, 80, 85, 92, 95, and 100 percent of the Freon equivalent design tip speed for the first rotor. The range of flow conditions extended from the maximum possible at wide-open throttle at each speed to the flow where surge was encountered. All tests were conducted at inlet stagnation pressures ranging from approximately 17 to 7 inches of mercury absolute. Reynolds numbers based on the mean radius chord of rotor 1 ranged from just above 1 million to almost 2.5 million.

RESULTS AND DISCUSSION

Overall Performance in Freon

The overall performance characteristics of the compressor are presented in figure 11. Overall stagnation pressure ratio is plotted against corrected weight flow for corrected speeds of from 40 to 100 percent of the Freon equivalent design speed for the first rotor, hereafter referred to as the design speed. Contours of constant efficiency based on measured exit total pressures are included. At design speed a peak pressure ratio of 3.12 (average total pressure ratio of 1.461 per stage) was obtained at a Freon corrected weight flow of 72.8 lb/sec (corresponding to an air equivalent specific weight flow based on the same inlet axial Mach number of 27.7 pounds per second per square foot of frontal area) and an efficiency of 0.82. The peak efficiency obtained at design speed was 0.83 and efficiencies of as high as 0.82 occurred for pressure ratios ranging from 2.65 to 3.12. It is difficult to place a meaningful single design point on the Freon performance grid (fig. 11) because of the previously mentioned differences in Freon and air density and pressure ratios for the same turning angles. The pressure ratio which results at the Freon equivalent conditions of rotor 1 from the mean radius calculation (fig. 9) for $V_{ai,E}$ and N_E is presented by a cross on figure 11. It has the last stator operating 9.3° above the design angle-of-attack condition. The dotted curve represents pressure ratios at this same N_E but computed by increasing the V_{ai} in order to reduce the 9.3° . This computed curve gives an order of magnitude for Freon conditions which are somewhat comparable to the original air design values. The maximum weight flow at design speed was 4 percent less than the Freon equivalent design weight flow indicated by the cross in figure 11. The vertical characteristic at this flow indicated that the back end of the compressor was choked. This choked condition will result if the early stages do not produce sufficient pressure ratio. In the detailed stage static-pressure ratios to be discussed in a later section, it will be seen that at design speed the first stage pressure ratio is much below the design value. Hence, the compressor was able to accommodate only 0.96 of the Freon equivalent design weight flow.

The highest overall pressure ratio and weight flow conditions for which an efficiency of 0.90 was obtained occurred at 0.92 of design speed (corresponding to approximately 1,100 ft/sec in air) where a pressure ratio of approximately 2.54 (1.364 per stage) was obtained at a corrected weight flow of 71.3 lb/sec (air equivalent specific weight flow is 27.1 pounds per second per square foot of frontal area).

The detailed efficiencies are presented in figure 12. For comparison purposes the efficiencies computed by the method of reference 16 in

which discharge stagnation pressure is computed from discharge static pressure and weight flow, are indicated by the dashed curves. A 3 to 5 percent decrease in peak efficiency results when efficiencies computed by this method are compared with those computed using measured discharge stagnation pressures. Part of this decrease results because this compressor was not designed with an axial discharge. A design point calculation indicated that ignoring design discharge swirl will result in a 2 percent decrease in efficiency. All efficiencies mentioned in describing the compressor performance will be those determined from measured discharge stagnation pressures. Peak efficiency gradually increased from 0.89 to 0.92 from 0.40 to 0.85 of the design speed. It remained high over most of the speed range dropping to just below 0.87 at 0.95 of design speed. As seen in figure 11 constant efficiency contours include a wide range of pressure ratio conditions at each speed.

The compressor exit Mach number variation with corrected weight flow and speed is presented in figure 13. Exit Mach number was obtained from outer casing static taps and measured discharge stagnation pressure. The surge line represents the minimum exit Mach numbers at which the compressor can operate without surging over the speed range. As compressor speed is increased the exit Mach number at the surge line is increased. This variation in exit Mach number indicates that the exit velocity increases more rapidly than either the speed of sound or the static temperature over the entire speed range. The rate of increase is more rapid from 0.40 to 0.80 of N_d than from 0.80 to 1.0 N_d . The value of air design exit Mach number at the tip section is indicated at the Freon equivalent weight flow for comparison purposes.

Stage Performance

The performance of the individual stages can be investigated by an examination of the outer casing static-pressure measurements. The stage static-pressure ratios obtained from these measurements have been plotted against corrected weight flow over the test speed range (fig. 14). The air-design tip section stage pressure ratios are indicated by dashed lines. On an individual stage basis neglecting multistage accumulative effects the corresponding Freon pressure ratios would be somewhat less (fig. 6(a)). At design speed the first stage developed considerably less static-pressure ratio than either the air design value or the peak values at 0.92 N_d , indicating a severe fall off in first stage performance at design speed. A comparison of the rotor inlet conditions at the maximum measured weight flow at design speed and the design values is presented in figure 15. The inlet relative Mach number at the tip was 1.22 compared with the design value of 1.24. The angle of attack was some 1.5° above the design value. Since the blade setting angles of rotor 1 were set using equivalent velocity diagrams, the blading is

actually operating at from 1.3° at the tip to 1.6° at the hub below the low-speed cascade design angles of attack at the design point. Hence, the measured weight-flow condition is actually very close to the design angles of attack as indicated by low-speed cascade tests. Evidently, the tip section combination of high design inlet Mach number, subsonic type of thickness distribution, moderately large maximum thickness (6 percent maximum thickness is fairly thick for transonic tip sections at $M_{iR} = 1.24$), and the design loading level has resulted in a rather inefficient tip region for the first rotor at design speed. It should further be stated that peak efficiency at this Mach number level might occur at angles of attack which are greater than low-speed cascade design angles of attack. It is the low-pressure ratio out of the first stage which resulted in the rear end of the compressor choking at less than the design weight flow.

At $0.92 N_d$, on the basis of the high peak compressor efficiency of 0.90 and the increased first-stage pressure ratio compared with its performance at N_d , it is obvious that first-stage performance has improved considerably over what occurred at design speed. The Mach number and inlet-angle conditions at the compressor peak efficiency point at $0.92 N_d$ are indicated in figure 15 for $\frac{W\sqrt{\theta\pi}}{\delta} = 71.4$ lb/sec. Hence, efficient multistage compressor performance was obtained for first rotor tip Mach numbers as high as 1.13. The first two stages appear to be fairly well matched at $0.92 N_d$ but the third stage is operating on the low flow side of the peak pressure ratio point over most of the weight-flow range (fig. 14). At $0.85 N_d$, all three stages appear to be well matched since they are all operating in the portion of their characteristic curves where efficiency is generally high. It was shown in a previous section concerned with the matching differences between an air design and Freon tests that, for identical inlet-angle conditions relative to rotor 1, a fairly good match point for a Freon test would occur some 6 percent below the Freon equivalent speed for rotor 1, provided, of course, the compressor was perfectly matched in air at the design point. On this basis, since all three stages are matched in the Freon tests at $0.85 N_d$, a similar match condition should exist for an air test at approximately 0.91 of the air design speed of 1,200 ft/sec. Since the Freon test results showed only a small decrease in peak efficiency between 0.85 and $0.91 N_d$, it was felt that the air test peak efficiency at $0.91 N_d$ should be near the 0.92 value obtained at $0.85 N_d$ in the Freon tests. A match point might occur somewhat above 0.91 of the air design speed condition in an air test since it is difficult to determine from the Freon tests how much above $0.85 N_d$ match conditions existed. It is necessary to limit the discussion of high efficiency match points that would occur in air tests to 0.95 of the air design speed. At this speed

and above it is first rotor performance which limits high efficiency performance and the Freon test results indicate that first rotor performance is falling off at this speed level.

As speed is decreased in figure 14 the weight flow of the compressor continues to be limited by the last stage which tends to operate near its choke condition. Hence, at all speeds, flow was limited by choked conditions of the last stage.

Radial Variation in Overall Stagnation Pressure Ratio

The radial variations in overall stagnation pressure ratio for 0.50, 0.85, 0.92, and 1.00 N_d at wide-open throttle setting, peak efficiency, and peak pressure ratio for each speed are presented in figure 16. At design speed the air design pressure ratio is indicated by a solid horizontal line. Over the entire speed range pressure ratio increases from hub to tip although the compressor was designed for constant power input from hub to tip. The increase is almost linear for peak efficiency at the highest two speeds. It should be noted that at wide open throttle conditions (the highest flow condition for each speed), the hub region invariably indicates a greater drop off in pressure ratio with respect to the rest of the annulus than occurs at the peak efficiency and peak pressure ratio conditions.

SUMMARY OF RESULTS

The following results were obtained from an investigation of the overall performance of a three-stage transonic axial-flow compressor that was tested in Freon-12:

1. The maximum stagnation pressure ratio obtained at the Freon equivalent of the air design speed was 3.12 at 72.8 lb/sec (corresponding to an air equivalent specific weight flow based on the same inlet axial Mach number of 27.7 pounds per second per square foot of frontal area) with an efficiency of 0.82.
2. The peak efficiency at the Freon equivalent design speed was 0.83 and efficiencies of as high as 0.82 occurred for pressure ratios ranging from 2.65 to 3.12.
3. The maximum weight flow obtained at design speed was 4 percent less than the Freon equivalent design weight flow.

4. Peak efficiency gradually increased from 0.89 to 0.92 from 0.40 to 0.85 of the Freon equivalent design speed. It remained high over most of the speed range dropping to just below 0.87 at 0.95 of Freon equivalent design speed.

5. The highest overall pressure ratio and weight flow for which an efficiency as high as 0.90 was obtained occurred at 0.92 of the Freon equivalent design speed (corresponds to approximately 1,100 ft/sec in air) where a pressure ratio of 2.54 (1.364 per stage) was obtained at a corrected weight flow of 71.3 lb/sec. (Air equivalent specific weight flow is 27.1 pounds per second per square foot of frontal area.)

6. At 0.85 of the Freon equivalent design speed, all three stages appear to be well matched. The efficiency level (0.90 to 0.92) at this match point is considered to be representative of the performance that should be obtained in an air test at 0.91 of the air design speed.

The following results were obtained from an analysis of the effects of using either air or Freon as the test medium for isentropic flow processes through a compressor blade row for the same inlet conditions (Mach number and inlet angle) and turning angles:

1. Pressure ratio in Freon is less than that in air while density ratio in Freon is greater than that in air.

2. Blade loading, expressed as overall static pressure rise in percent of the difference between inlet stagnation and static pressure, was approximately the same for inlet Mach numbers up to 0.80 and pressure ratios as high as 1.6 with the possibility of considerably greater loadings in Freon than in air for higher inlet Mach numbers.

3. Freon efficiencies may actually be conservative when considered to be a measure of the efficiency of the corresponding air test at the same inlet conditions of Mach number and inlet angle.

4. The use of Freon as the test medium for high-pressure ratio multistage compressors, which have considerably higher overall pressure ratios than the compressor reported herein and which are designed for air operation, is considered to be undesirable because of stage mismatching which results because density rises in Freon are different from those which occur in air.

Langley Aeronautical Laboratory,
National Advisory Committee for Aeronautics,
Langley Field, Va., July 21, 1955.

APPENDIX A
 DERIVATION OF EQUATIONS USED TO COMPUTE
 VELOCITIES FOR VELOCITY DIAGRAMS

At any radial station between blade rows

$$t = T - \frac{V^2}{2c_p} \quad (A1)$$

and the differential of this expression is

$$dt = dT - \frac{VdV}{c_p} \quad (A2)$$

The fundamental energy equation states that

$$\frac{dp}{\rho} = c_p dt \quad \text{for } ds = 0 \quad (A3)$$

Therefore, equation (A2) for $ds = 0$ radially becomes

$$\frac{dp}{\rho} = c_p dT - VdV \quad (A4)$$

Assuming that simple radial equilibrium holds

$$\frac{dp}{\rho} = \frac{V_T^2}{r} dr \quad (A5)$$

Substitution of equation (A5) into (A4) results in

$$V dV = c_p dT - \frac{V_T^2}{r} dr \quad (A6)$$

Integration of equation (A6) between any two radial stations B and C results in

$$V_B^2 - V_C^2 = 2c_p(T_B - T_C) - 2 \int_{r_C}^{r_B} \frac{V_T^2}{r} dr \quad (A7)$$

For the condition of all stages having radially constant power input, if the velocities are presented in component form neglecting any radial components, equation (A7) becomes

$$V_{a,B}^2 - V_{a,C}^2 = V_{T,C}^2 - V_{T,B}^2 - 2 \int_{r_C}^{r_B} \frac{V_T^2}{r} dr \quad (A8)$$

This equation can be written between any two radial stations. If station C is arbitrarily selected to be at the mean radius station denoted by m , and B is any other radial station equation (A8) becomes

$$V_a^2 - V_{a,m}^2 = (V_{T,m}^2 - V_T^2) - 2 \int_{r_m}^r \frac{V_T^2}{r} dr \quad (A9)$$

Satisfaction of Continuity

Equation (A9) yields the radial variation in axial velocity for any tangential velocity distribution. To obtain the actual velocity values requires the satisfaction of the continuity equation

$$W = 2\pi \int_{r_h}^{r_t} \rho V_a r dr \quad (A10)$$

Hence, if the hub-tip ratio is specified, the final computation of axial velocities resolves itself into a trial and error solution in which the selection of $V_{a,m}$ in equation (A9) is altered until equation (A10) is satisfied.

Another method of utilizing equations (A9) and (A10) to obtain the velocities between blade rows is to specify an axial velocity change across a blade row at some radial station such as the tip section. This

action is similar to setting the tip section loading. Axial velocities can then be determined from equation (A9) written between the tip and any other radial station. The hub radius is then determined by solving equation (A10) for r_h . This method has the desirable feature that it eliminates a trial and error solution of equation (A10) for $V_{a,m}$ and also permits a tip section loading to be set directly.

The computational method used in the design of the compressor herein reported was to compute velocities from the previously described equations for a prescribed inner contour. An approximate method of determining the $V_{a,m}$ in equation (A9) that would satisfy equation (A10) was used. It was assumed that the mean radius conditions at blade row inlet and exit stations represented average conditions. Downstream $V_{a,m}$ and ρ_m were computed from inlet and exit passage areas and the inlet mean radius axial velocities and densities, that is, from $(\rho_i V_{ai})_m A = (\rho V_a)_m A$.

After the satisfaction of continuity (equation (A10)) by the above method, the hub casing radii were arbitrarily reduced to account for casing boundary-layer growth. This reduction in area is similar to assuming boundary-layer blockage factors ($K = W_d/W_{ideal}$). A tabulation of the corresponding K factors is presented in table II. To determine the effective boundary-layer blockage factors that resulted from the actual hub radii, the assumed K factors, and the approximate method of satisfying continuity that was used, W_{ideal} was computed at each axial station by a numerical integration of the calculated weight-flow distributions. The hub radii used in these integrations were the actual hub radii. A tabulation of the effective K 's is presented in table II. The fact that some of the K values are greater than 1.00 resulted because the previously mentioned approximate method used to satisfy continuity yielded weight flows which were from 1 to 1.5 percent below the design value. At the time this compressor was designed, very little information was available regarding what values of K to use. Hence, a redesign of the compressor to provide a smooth decrease in effective K values from inlet to exit was considered to be unnecessary. It was also felt that the increase in angles of attack which would result in the third stage for K values above unity would not exceed the high efficiency angle-of-attack range of that stage.

APPENDIX B

THE EFFECT OF TEST FLUID ON PERFORMANCE OF A BLADE ROW

A comparison between the performance of a blade row in air ($\gamma = 1.4$) and Freon-12 ($\gamma = 1.25$) will be made for isentropic flow conditions. It is assumed that the blade row turning angle is independent of the test fluid. The subscript F will refer to Freon-12 as the test fluid, and no subscript refers to air. The comparisons will be made at the same inlet conditions in each fluid, that is, the same M_i , β_i , and P_i . The flow processes will be assumed to be isentropic. Hence, $P_i = P_e = P$ and $A_{cr_i} = A_{cr_e} = A_{cr}$. At the inlet:

$$\frac{P}{P_i} = \left(1 + \frac{\gamma - 1}{2} M_i^2\right)^{\frac{\gamma}{\gamma - 1}} \quad (B1)$$

and

$$\frac{A_i}{A_{cr}} = \frac{1}{M_i} \left[\frac{2}{\gamma + 1} \left(1 + \frac{\gamma - 1}{2} M_i^2\right) \right]^{\frac{\gamma + 1}{2(\gamma - 1)}} \quad (B2)$$

$\frac{P}{P_i}$ and $\frac{A_i}{A_{cr}}$ are determined for M_i . $\frac{P}{P_e}$ is then obtained by multiplying $\frac{P}{P_i}$ by $\frac{P_i}{P_e}$ which is known. M_e is then determined from equation (B1) written at the exit station. $\frac{A_e}{A_{cr}}$ is determined by solving equation (B2) written at station e. $\frac{A_i}{A_e}$ is determined from $\frac{A_i}{A_{cr}}$ and $\frac{A_e}{A_{cr}}$.

Since on a one-dimensional basis

$$\frac{A_i}{A_e} = \frac{\cos \beta}{\cos(\beta - \theta)} \quad (B3)$$

and β and θ are assumed to be the same regardless of the test fluid,

$$\frac{A_i}{A_e} = \left(\frac{A_i}{A_e} \right)_F \quad (B4)$$

From $M_i = M_{i,F}$ the value of $\left(\frac{A_i}{A_{cr}} \right)_F$ can be determined from equation (B2) written for Freon inlet conditions. From this area ratio and equation (B4), $\left(\frac{A_e}{A_{cr}} \right)_F$ was computed. The Freon value of exit Mach number, $M_{e,F}$ is determined by writing equation (B2) for Freon exit conditions and solving it using the value of $\left(\frac{A_e}{A_{cr}} \right)_F$ computed. Since M_i and M_e in both air and Freon have been determined, the comparisons of Freon and air static pressure ratio, static density ratio, and loading parameter expressed as $\frac{p_e - p_i}{(P - p)_i}$ are determined from the following equations:

$$\frac{p_e}{p_i} = \left[\frac{1 + \frac{\gamma - 1}{2} M_i^2}{1 + \frac{\gamma - 1}{2} M_e^2} \right]^{\frac{\gamma}{\gamma - 1}} \quad (B5a)$$

and

$$\left(\frac{p_e}{p_i} \right)_F = \left[\frac{1 + \frac{\gamma_F - 1}{2} M_i^2}{1 + \frac{\gamma_F - 1}{2} M_{e,F}^2} \right]^{\frac{\gamma_F}{\gamma_F - 1}} \quad (B5b)$$

Hence $\left(\frac{p_e}{p_i} \right) / \left(\frac{p_e}{p_i} \right)_F$ is obtained by dividing equation (B5a) by (B5b).

$$\frac{p_e}{p_i} / \left(\frac{p_e}{p_i} \right)_F = \left(\frac{p_e}{p_i} \right)^{\frac{1}{\gamma}} / \left(\frac{p_e}{p_i} \right)_F^{\frac{1}{\gamma_F}} \quad (B6)$$

and

$$\frac{p_e - p_i}{(P - p)_i} \bigg/ \frac{(p_e - p_i)_F}{(P - p)_{i,F}} = \left(\frac{\frac{p_e}{p_i} - 1}{\frac{P}{p_i} - 1} \right) \bigg/ \left(\frac{\left(\frac{p_e}{p_i} \right)_F - 1}{\left(\frac{P}{p_i} \right)_F - 1} \right) \quad (B7)$$

where p_e/p_i is determined from equation (B5a), $(p_e/p_i)_F$ from (B5b), P/p_i from (B1), and $(P/p_i)_F$ from (B1) written for Freon.

The comparative computations were made for various combinations of inlet Mach number and air static pressure ratios. As mentioned previously, all calculations were done isentropically which means that all flow processes were treated as shockless. Hence, for the conditions computed for inlet Mach numbers above 1.0 no account of shock losses was made. Whenever the air condition went from supersonic inlet to subsonic exit flow conditions to produce a given pressure ratio the corresponding Freon condition was assumed to do likewise.

REFERENCES

1. Sandercock, Donald M., Lieblein, Seymour, and Schwenk, Francis C.: Experimental Investigation of an Axial-Flow Compressor Inlet Stage Operating at Transonic Relative Inlet Mach Numbers. IV - Stage and Blade-Row Performance of Stage with Axial-Discharge Stators. NACA RM E54C26, 1954.
2. Serovy, George K., Robbins, William H., and Glaser, Frederick W.: Experimental Investigation of a 0.4 Hub-Tip Diameter Ratio Axial-Flow Compressor Inlet Stage at Transonic Inlet Relative Mach Numbers. I - Rotor Design and Over-All Performance at Tip Speeds From 60 to 100 Percent of Design. NACA RM E53I11, 1953.
3. Savage, Melvyn, and Felix, A. Richard: Investigation of a High-Performance Axial-Flow Compressor Transonic Inlet Rotor Designed for 37.5 Pounds Per Second Per Square Foot of Frontal Area - Aerodynamic Design and Overall Performance. NACA RM L55A05, 1955.
4. Schwenk, Francis C., Lieblein, Seymour, and Lewis, George W., Jr.: Experimental Investigation of an Axial-Flow Compressor Inlet Stage Operating at Transonic Relative Inlet Mach Numbers. III - Blade-Row Performance of Stage With Transonic Rotor and Subsonic Stator at Corrected Tip Speeds of 800 and 1,000 Feet Per Second. NACA RM E53G17, 1953.
5. Kovach, Karl, and Sandercock, Donald M.: Experimental Investigation of a Five-Stage Axial-Flow Research Compressor With Transonic Rotors in All Stages. II - Compressor Over-all Performance. NACA RM E54G01, 1954.
6. Geye, Richard P., Budinger, Ray E., and Voit, Charles H.: Investigation of a High-Pressure-Ratio Eight-Stage Axial-Flow Research Compressor With Two Transonic Inlet Stages. II - Preliminary Analysis of Over-All Performance. NACA RM E53J06, 1953.
7. Klapproth, John F.: General Considerations of Mach Number Effects on Compressor-Blade Design. NACA RM E53L23a, 1954.
8. Herrig, L. Joseph, Emery, James C., and Erwin, John R.: Systematic Two-Dimensional Cascade Tests of NACA 65-Series Compressor Blades at Low Speeds. NACA RM L51G31, 1951.
9. Sandercock, Donald M., Kovach, Karl, and Lieblein, Seymour: Experimental Investigation of a Five-Stage Axial-Flow Research Compressor With Transonic Rotors in All Stages. I - Compressor Design. NACA RM E54F24, 1954.

10. Budinger, Raymond E., and Thomson, Arthur R.: Investigation of a 10-Stage Subsonic Axial-Flow Research Compressor. II - Preliminary Analysis of Over-All Performance. NACA RM E52C04, 1952.
11. Lieblein, Seymour, Schwenk, Francis C., and Broderick, Robert L.: Diffusion Factor for Estimating Losses and Limiting Blade Loadings in Axial-Flow-Compressor Blade Elements. NACA RM E53D01, 1953.
12. Erwin, John R., Savage, Melvyn, and Emery, James C.: Two-Dimensional Low-Speed Cascade Investigation of NACA Compressor Blade Sections Having a Systematic Variation in Mean-Line Loading. NACA RM L53I30b, 1953.
13. Savage, Melvyn, Felix, A. Richard, and Emery, James C.: High-Speed Cascade Tests of a Blade Section Designed for Typical Hub Conditions of High-Flow Transonic Rotors. NACA RM L55F07, 1955.
14. Boxer, Emanuel, and Erwin, John R.: Investigation of a Shrouded and an Unshrouded Axial-Flow Supersonic Compressor. NACA RM L50G05, 1950.
15. Von Doenhoff, Albert E., Braslow, Albert L., and Schwartzberg, Milton A.: Studies of the Use of Freon-12 as a Wind Tunnel Testing Medium. NACA TN 3000, 1953.
16. NACA Subcommittee on Compressors: Standard Procedures for Rating and Testing Multistage Axial-Flow Compressors. NACA TN 1138, 1946.

TABLE I
SUMMARY OF VELOCITY DIAGRAM DATA

Blade row	Inlet radius ratio, r_i/r_t	Exit radius ratio, r_e/r_t	Inlet Mach number, M	Inlet angle, β , deg	Turning angle, θ , deg	Axial velocity ratio, V_{ae}/V_{ai}	$\frac{\Delta p}{(P - p)_1}$	D-factor
R1	0.500	0.578	0.783	45.0	28.6	0.892	0.63	0.59
	.750	.789	.998	56.3	10.4	.892	.45	.46
	1.000	1.000	1.238	63.4	4.5	.892	.29	.34
S1	.606	.634	.676	41.8	30.2	1.000	.30	.41
	.803	.817	.602	34.0	18.8	.972	.19	.28
	1.000	1.000	.566	28.5	9.3	.935	.14	.18
R2	.657	.692	.805	46.4	30.0	1.040	.49	.53
	.829	.846	.909	53.4	15.9	.924	.48	.51
	1.000	1.000	1.021	59.2	6.0	.794	.43	.46
S2	.712	.744	.765	43.8	28.7	1.028	.43	.51
	.856	.872	.693	44.5	26.5	1.000	.36	.46
	1.000	1.000	.636	47.3	26.2	.966	.30	.42
R3	.750	.750	.797	49.3	28.4	.963	.50	.58
	.875	.875	.865	54.2	15.1	.849	.51	.56
	1.000	1.000	.935	58.6	4.9	.723	.47	.51
S3	.750	.750	.707	49.7	28.0	.814	.55	.61
	.875	.875	.640	51.3	25.0	.766	.52	.57
	1.000	1.000	.584	54.5	23.1	.706	.48	.54

TABLE II

INNER CONTOUR AND BOUNDARY-LAYER BLOCKAGE FACTORS

	Axial station, in.	Hub-tip ratio	Assumed K-factors	Effective K-factors
R1-i	0.00	0.500	1.00	1.00
R1-e	2.17	.575	.99	.99
S1-i	3.52	.602	.99	1.00
S1-e	5.25	.629	.99	1.00
R2-i	6.67	.651	.99	1.00
R2-e	8.85	.685	.98	.99
S2-i	10.00	.700	.97	.98
S2-e	11.90	.725	.95	.96
R3-i	13.05	.743	.97	.97
R3-e	15.16	.750	1.00	1.01
S3-i	16.32	.750	1.00	1.01
S3-e	18.14	.750	1.00	1.01

TABLE III

SUMMARY OF BLADE-SELECTION DATA

Blade row	$\frac{r_i + r_e}{2r_t}$	Inlet angle, β' , deg	Turning angle, θ' , deg	Blade section	Solidity, σ	Chord, c, in.	Blade setting angle, $\beta' - \alpha'$, deg	$\Delta\alpha'$, deg	$\Delta\alpha$, deg	$\Delta\theta'$, deg
R1	0.539	46.6	31.0	65(17.5A ₁₀)10	1.250	2.42	28.0	0	-1.6	0
	.770	57.7	13.4	65(8.5A _{6I4b})08	1.087	3.00	48.2	0	-1.3	0
	1.000	64.7	7.2	65(4.7A _{2I8b})06	1.000	3.59	59.0	0	-1.3	0
S1	.620	41.1	29.2	65(15.8A ₁₀)06	1.191	1.86	21.7	+2.7	+3.4	+1.6
	.810	33.8	18.3	65(9.9A ₁₀)08	1.045	2.13	22.4	+3	+5	-.2
	1.000	28.7	9.7	65(4.7A ₁₀)10	.953	2.40	23.9	-2.0	-2.2	-2.1
R2	.674	46.7	30.4	65(17.5A ₁₀)10	1.215	2.42	27.2	+1.2	+9	+1.3
	.837	54.9	19.0	Rest of blade obtained from rotor 1 master	1.145	2.83	42.7	0	-1.5	-1.3
	1.000	61.8	12.0		1.100	3.25	53.4	+1	-2.5	-1.3
S2	.728	44.6	30.0	65(16.9A ₁₀)06	1.195	2.18	27.4	-.4	-1.2	-.4
	.864	44.4	26.3	65(16.0A ₁₀)08	1.052	2.28	29.2	-.5	-.4	-.2
	1.000	45.7	23.6	65(15.3A ₁₀)10	.953	2.39	32.0	-.7	+9	-.6
R3	.750	50.5	30.6	65(17.5A ₁₀)10	1.220	2.42	30.4	+1.8	+6	+6
	.875	56.7	20.3	Rest of blade obtained from rotor 1 master	1.184	2.74	43.1	+1	-2.4	-.6
	1.000	62.2	13.3		1.154	3.05	51.9	+3	-3.3	+3
S3	.750	51.9	31.9	65(16.9A ₁₀)06	1.385	2.18	33.3	-.5	-2.7	-2.1
	.875	52.7	27.6	65(16.1A ₁₀)078	1.243	2.28	34.9	+5	-.9	+1
	1.000	54.9	23.7	65(15.4A ₁₀)096	1.135	2.38	37.3	+1.7	+1.3	+2.2

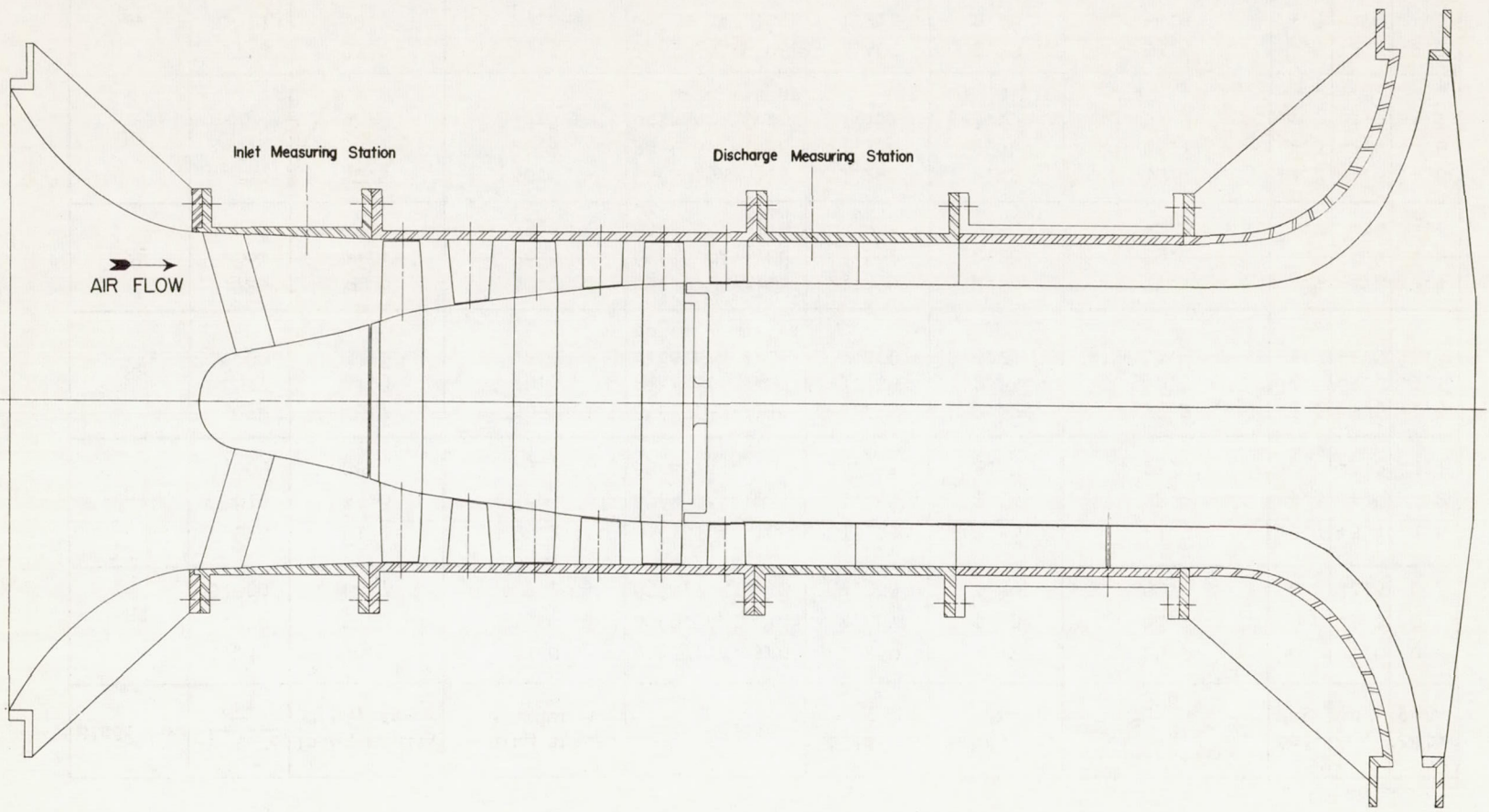
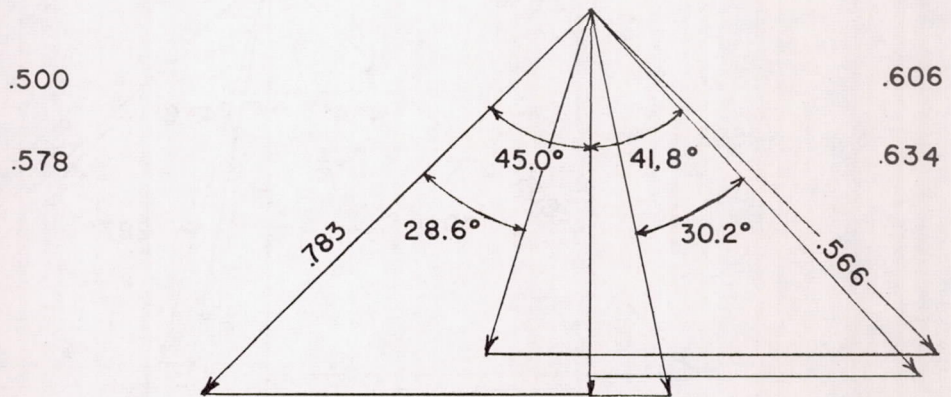
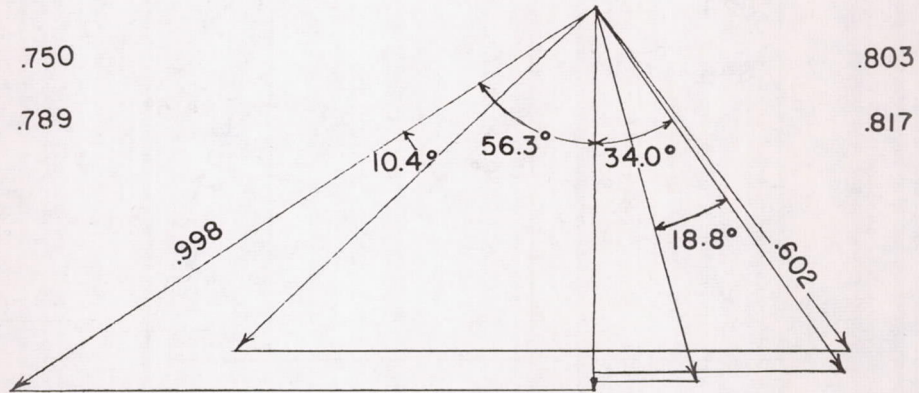
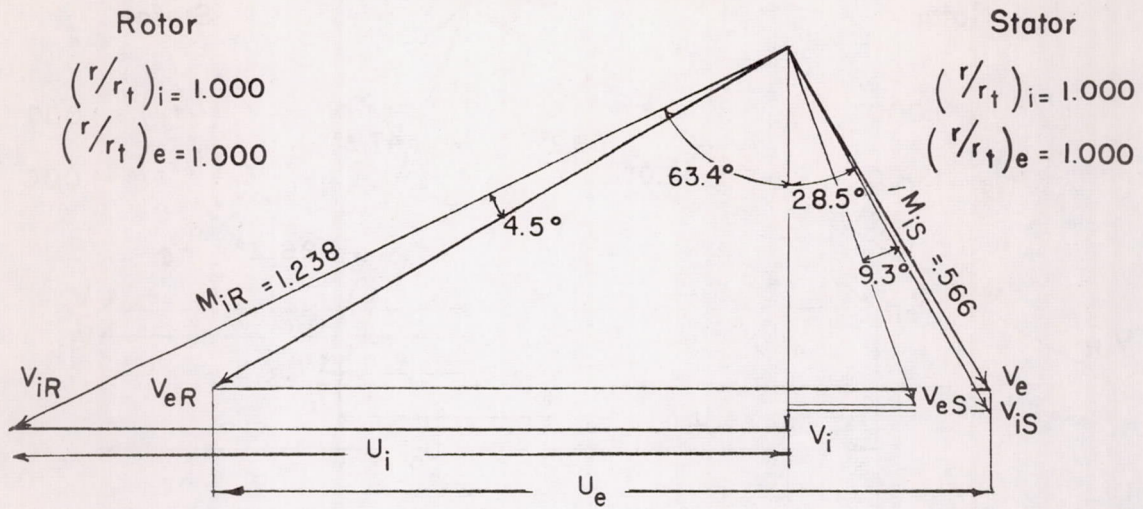
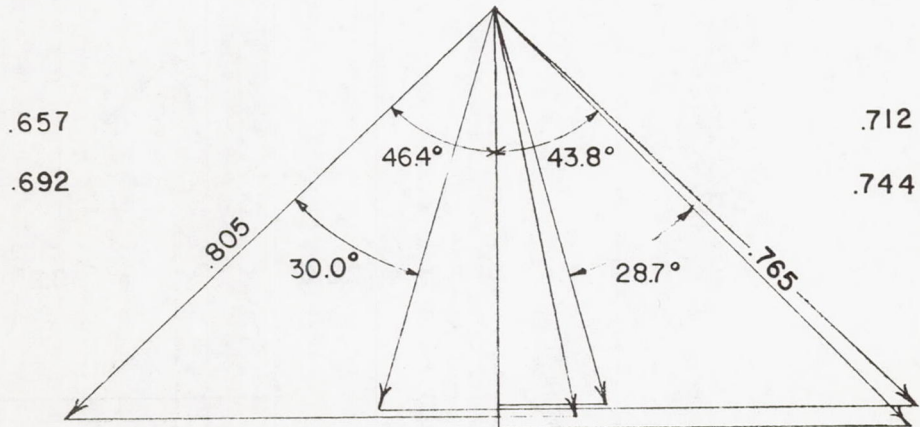
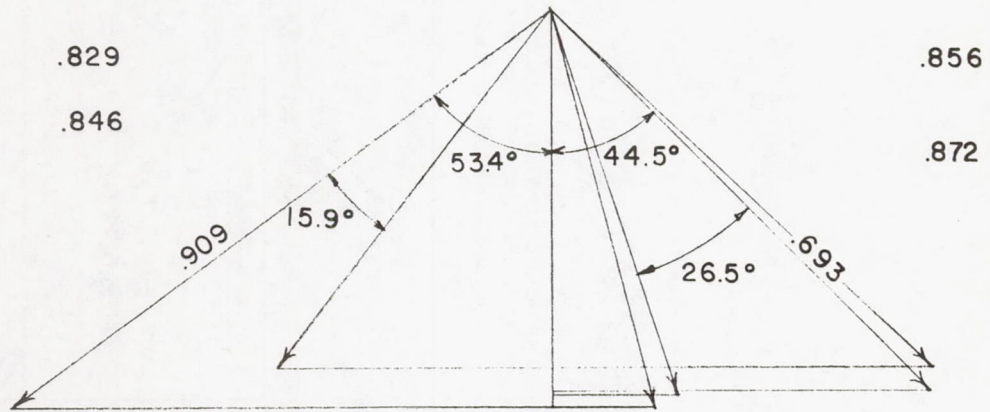
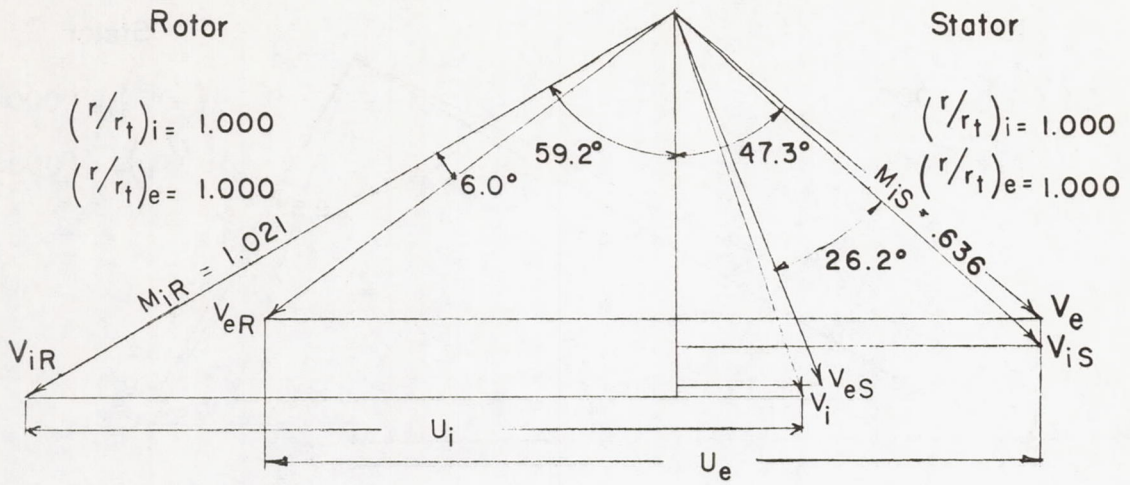


Figure 1.- Schematic drawing of three-stage transonic compressor.



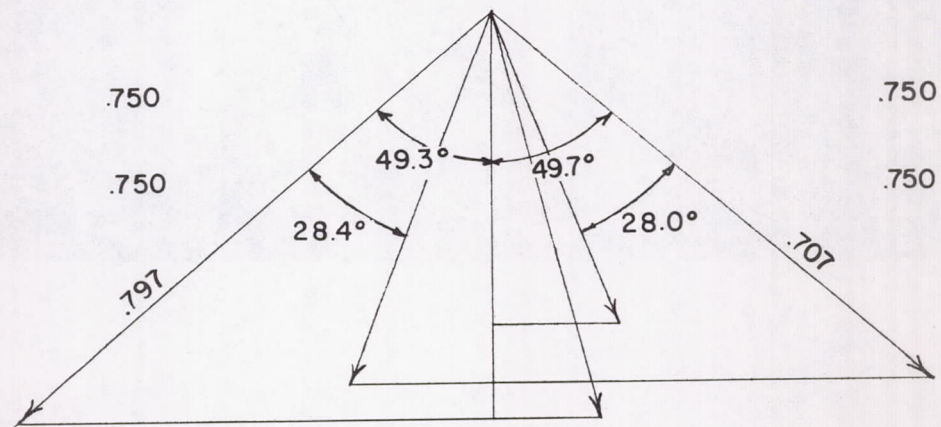
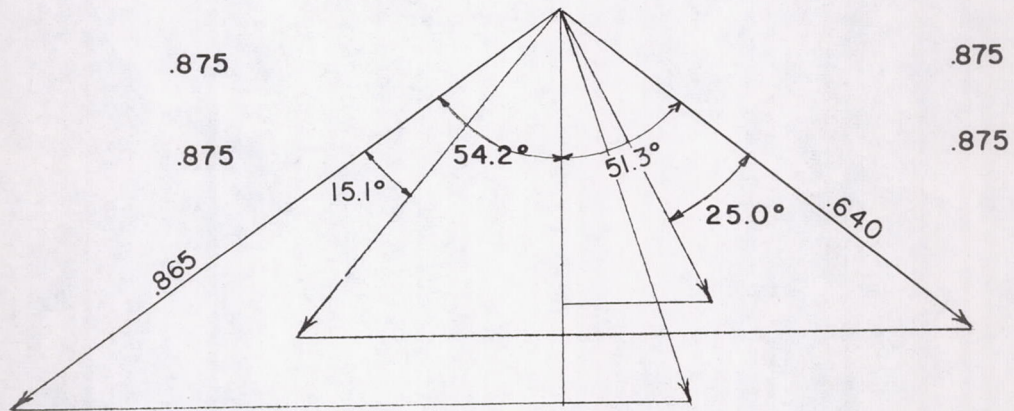
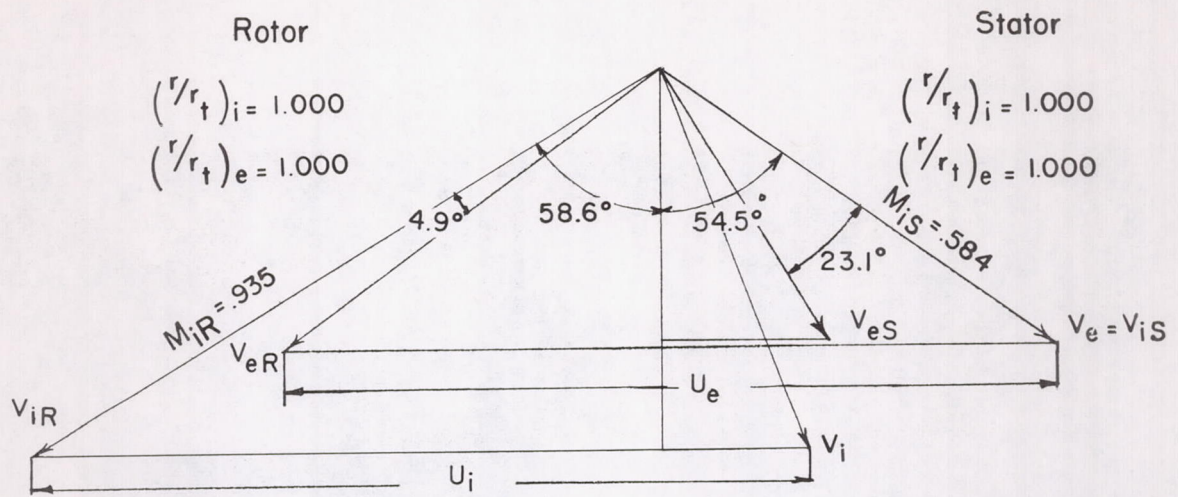
(a) First stage.

Figure 2.- Design velocity diagrams.



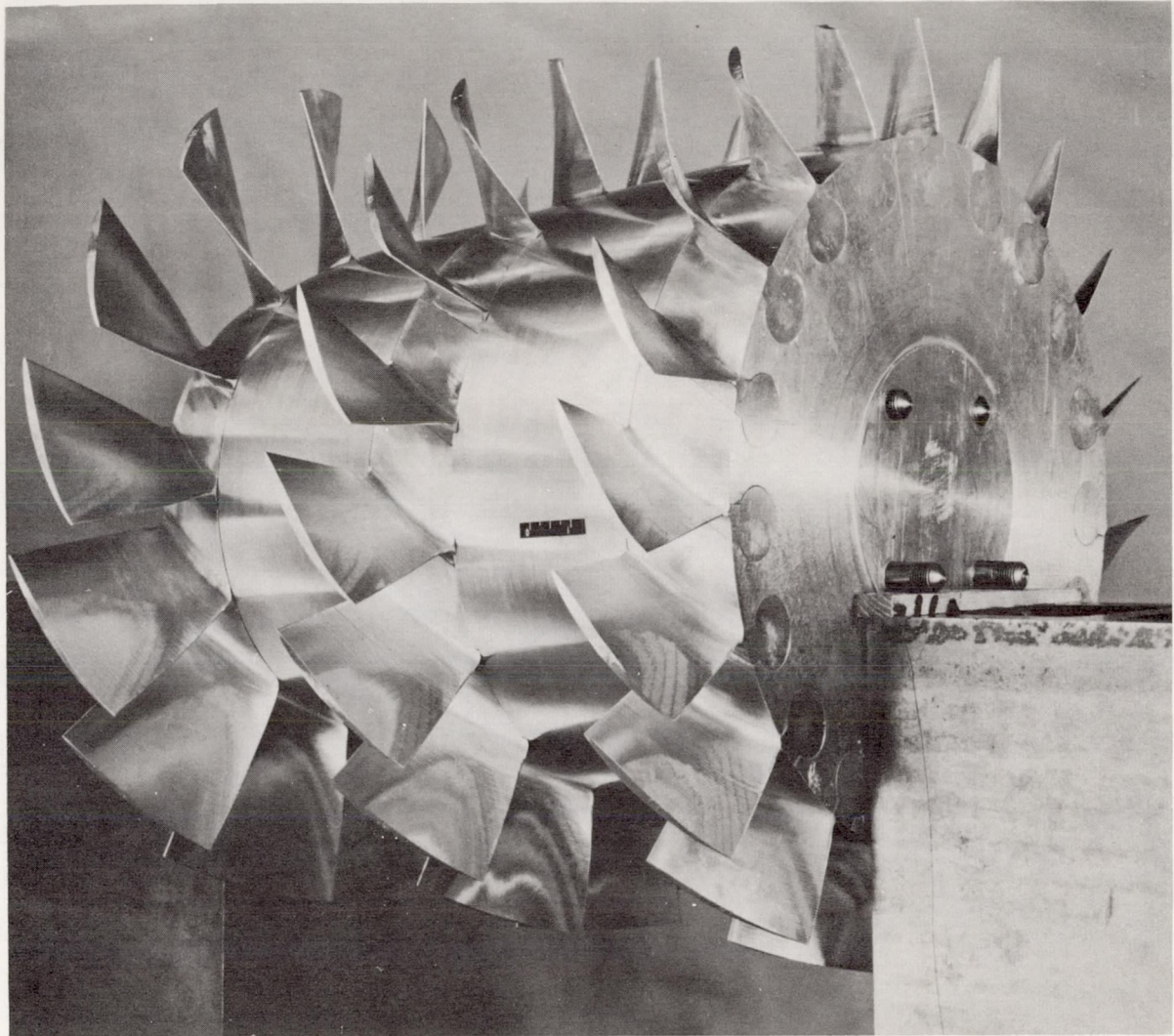
(b) Second stage.

Figure 2.- Continued.



(c) Third stage.

Figure 2.- Concluded.



L-79095

Figure 3.- Photograph of rotor assembly of three-stage transonic compressor.

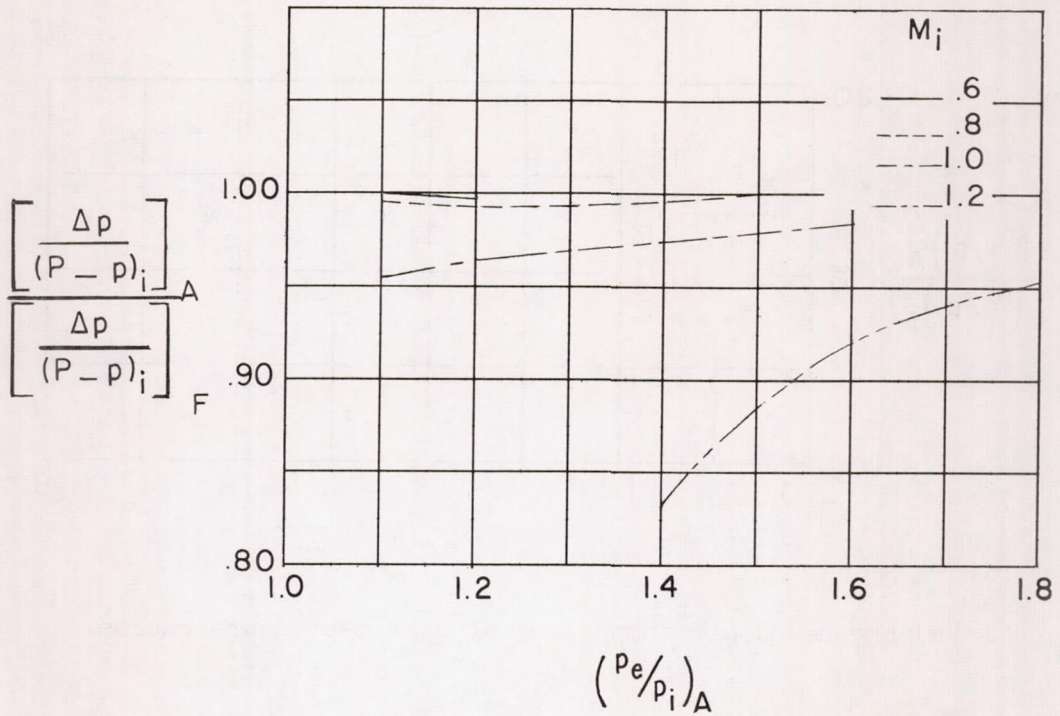


Figure 4.- Freon and air comparison of the blade loading expressed as $\frac{\Delta p}{(P - p)_i}$ across a blade row for various air static-pressure ratios and inlet Mach numbers. In the computations, inlet conditions and turning angles were the same for each of the two gases and flow processes were assumed to be isentropic.

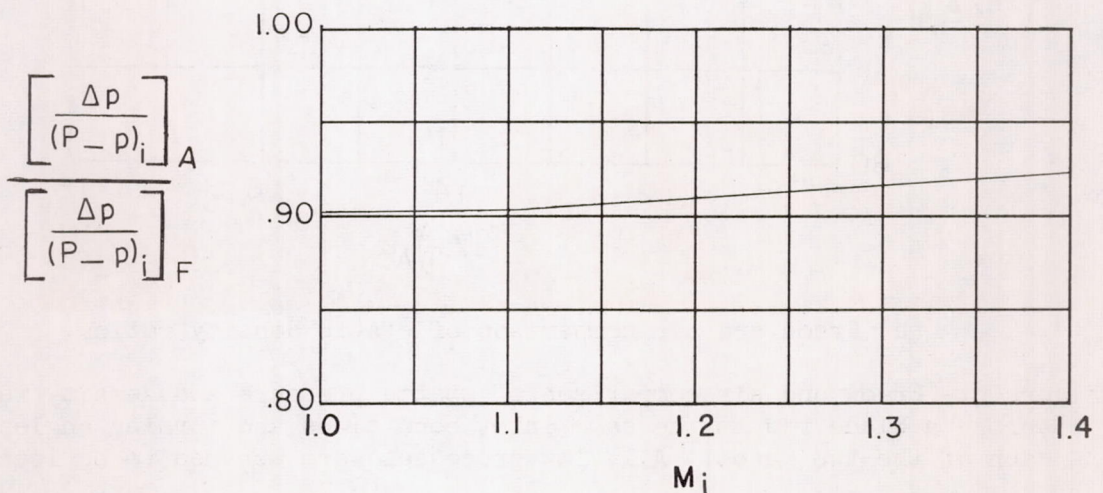
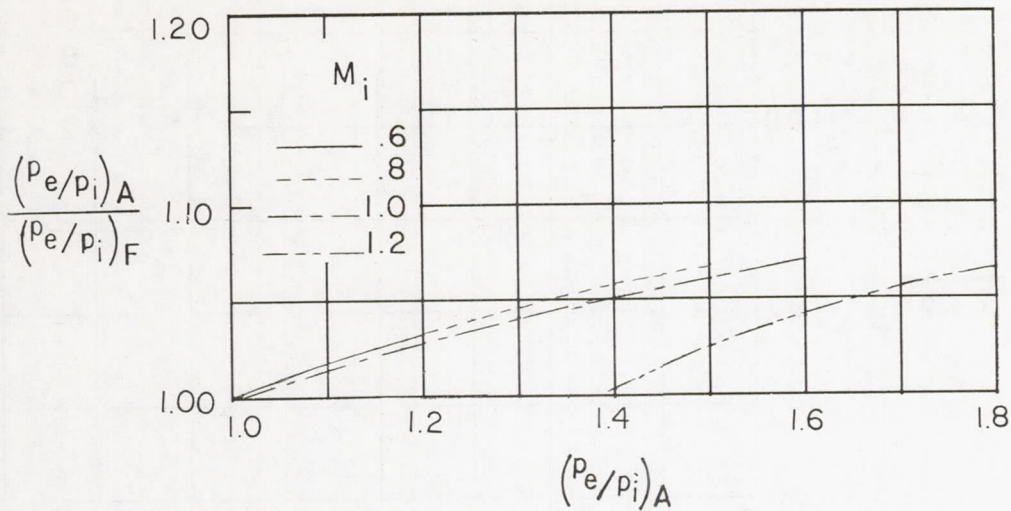
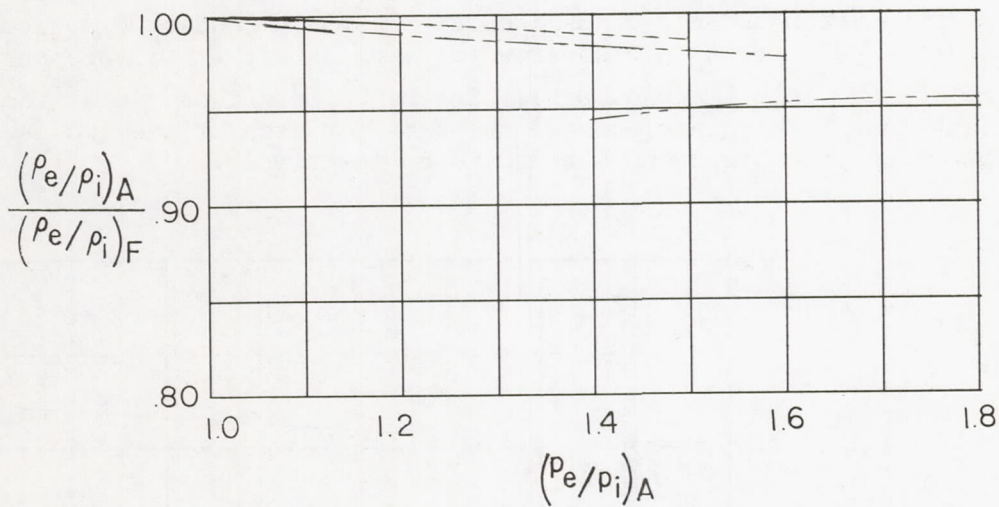


Figure 5.- Variation in pressure recovery across a normal shock for Freon and air with shock inlet Mach number.



(a) Freon and air comparison of static-pressure ratios.



(b) Freon and air comparison of static density ratios.

Figure 6.- Freon and air comparison of static pressure and density ratios across a blade row at the same inlet conditions and turning angles for each of the two gases. All flow processes were assumed to be isentropic.

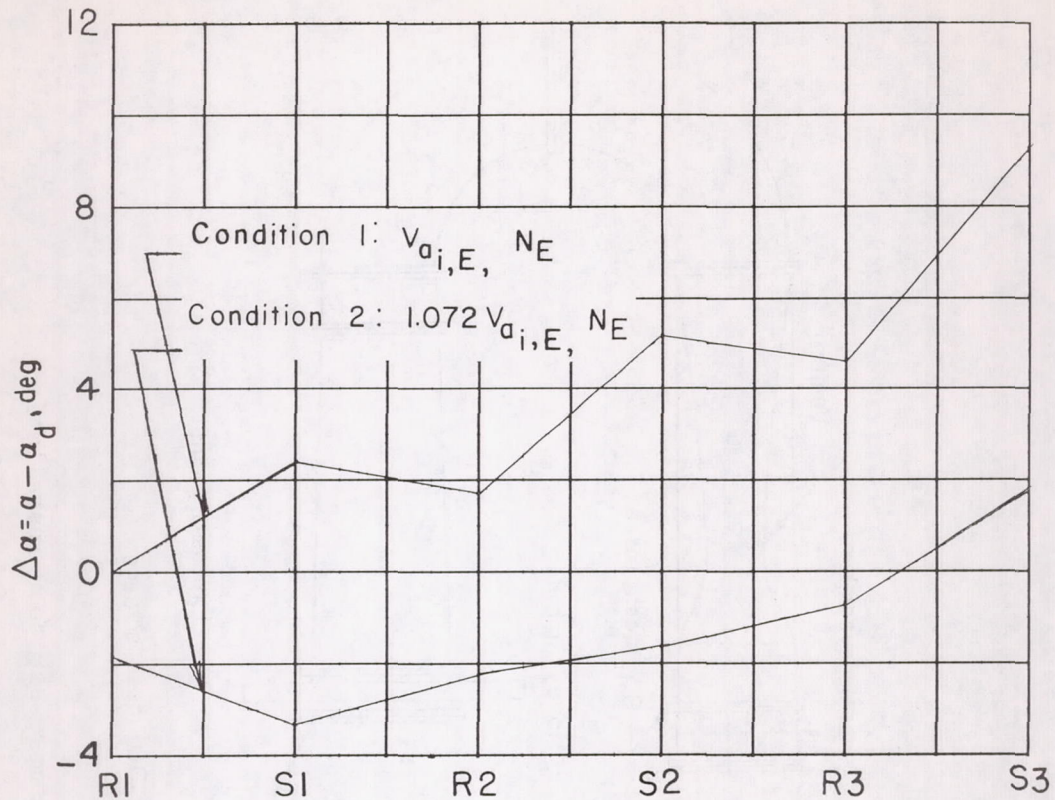


Figure 7.- Deviations from mean radius air design angles of attack through the compressor which result from one-dimensional calculations at conditions 1 and 2.

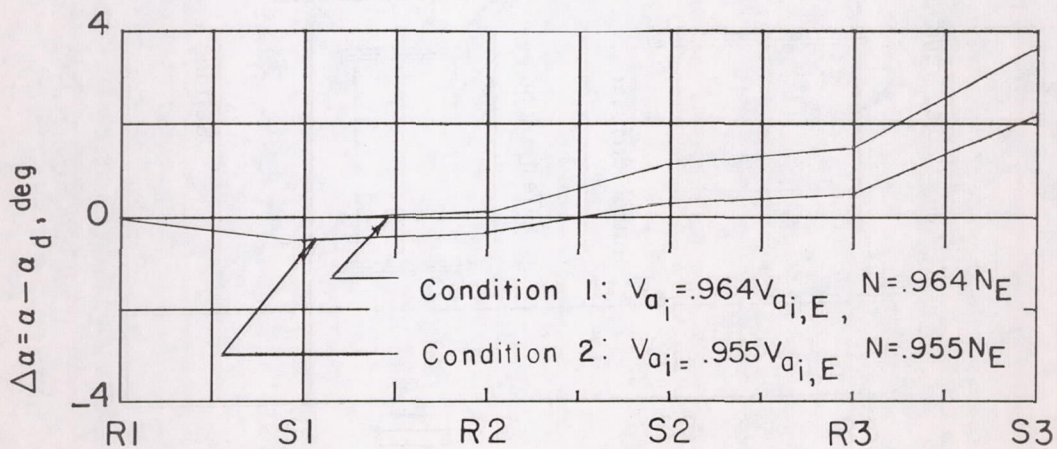


Figure 8.- Deviations from mean radius air design angles of attack through the compressor which result from one-dimensional calculations at conditions 1 and 2.

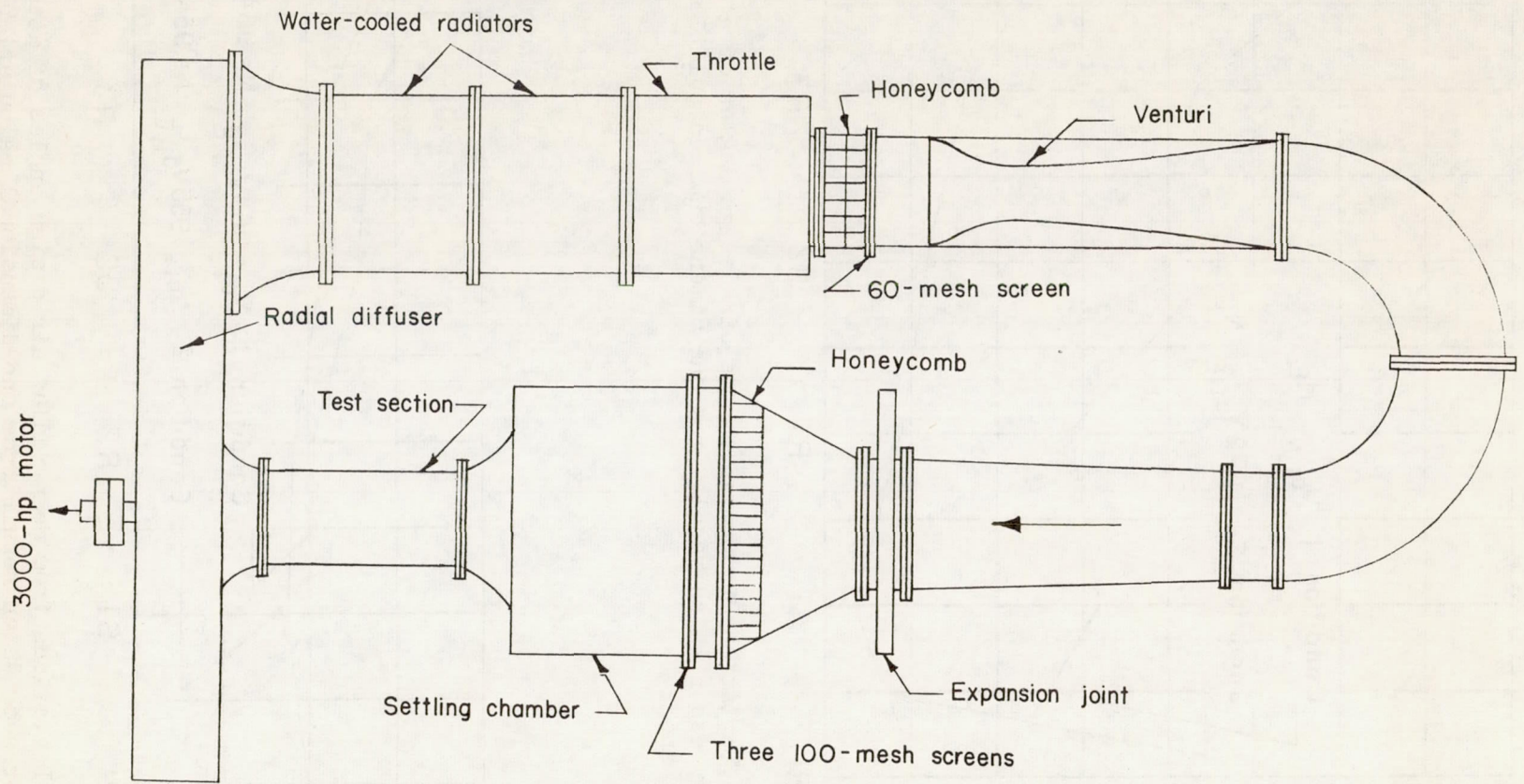
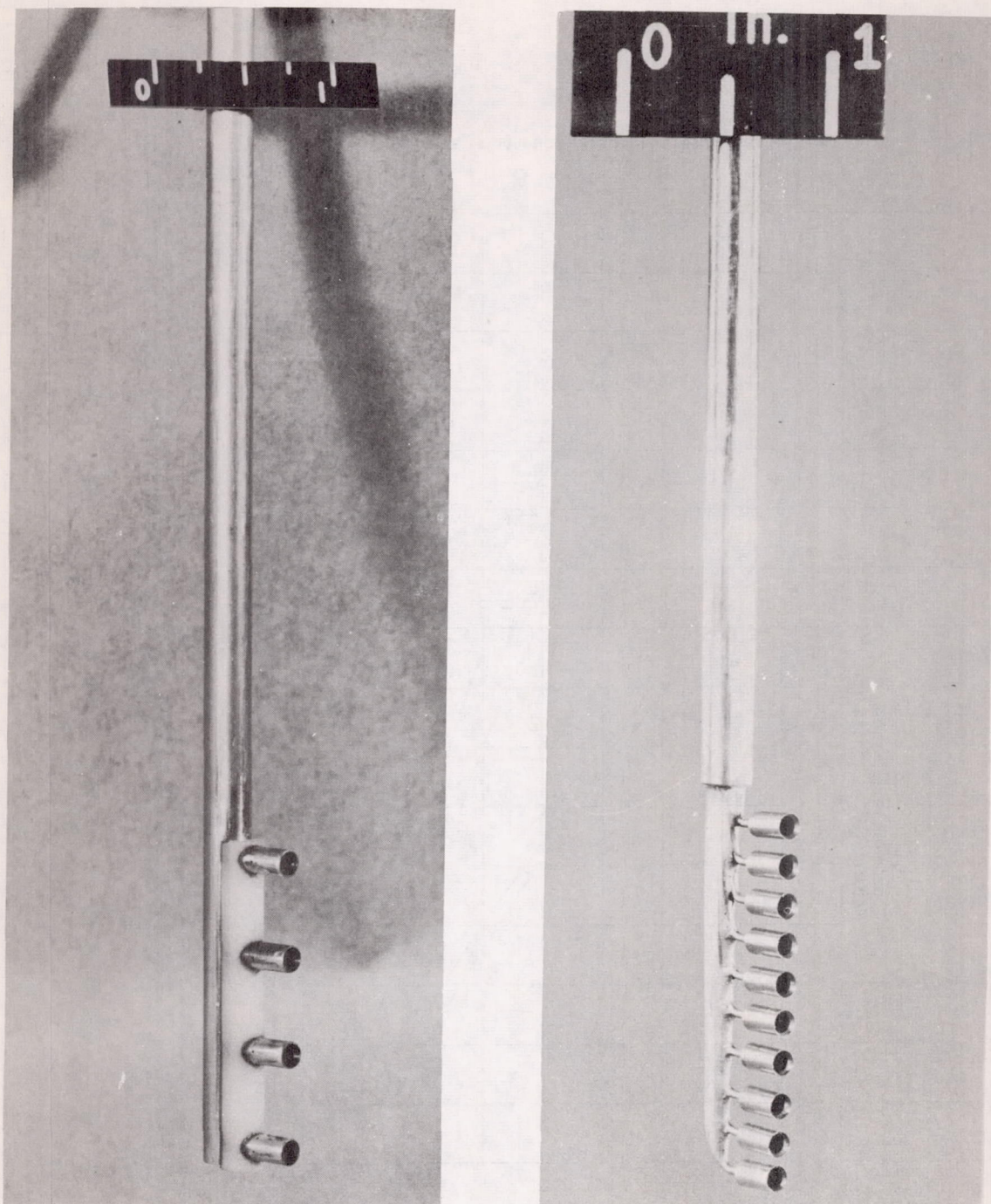


Figure 9.- Schematic diagram of compressor test installation.



L-89378

(a) Four-bell thermocouple rake.

(b) Ten-bell stagnation pressure rake.

Figure 10.- Stagnation pressure and temperature rakes.

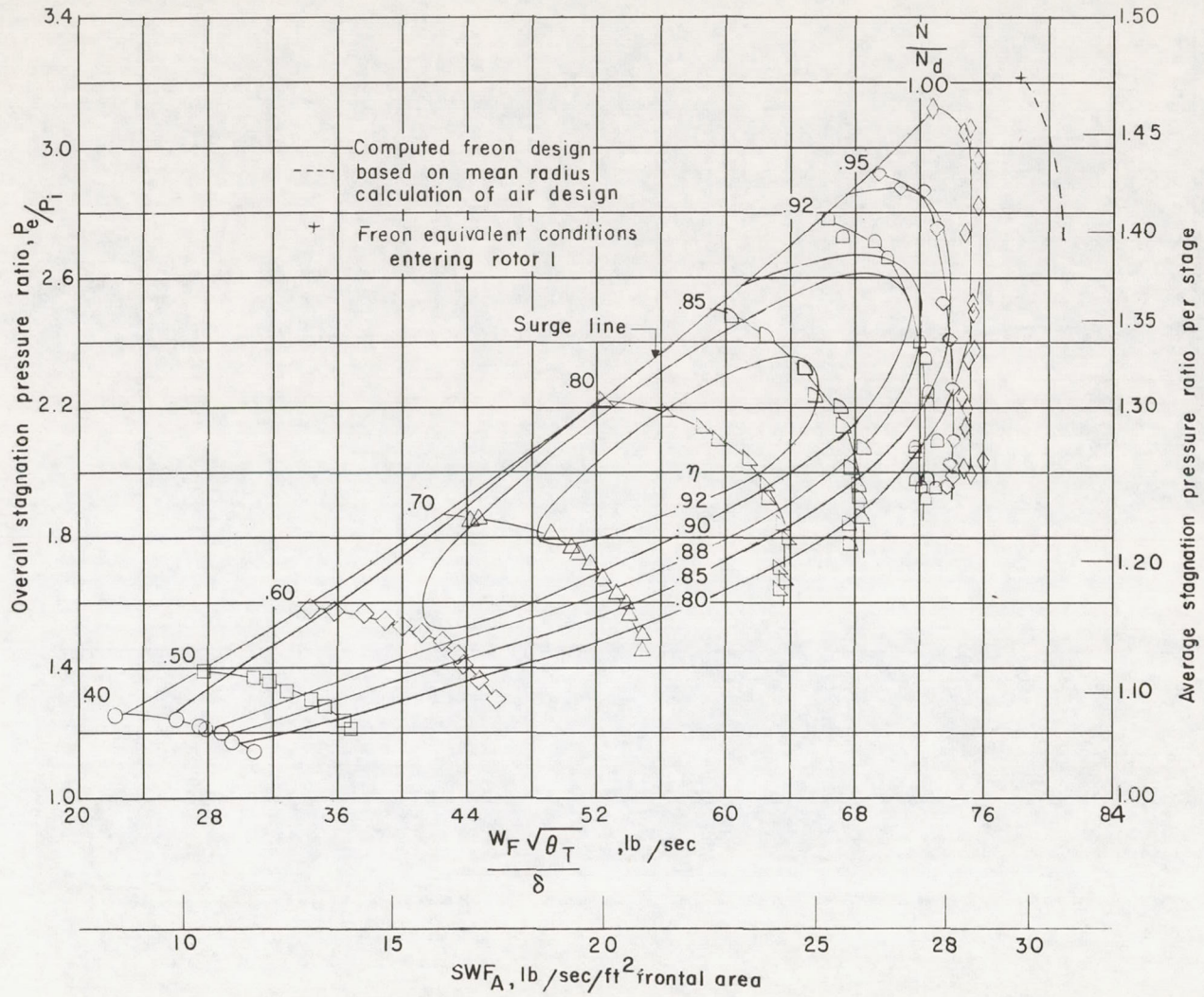


Figure 11.- Overall performance characteristics of the three-stage transonic compressor.

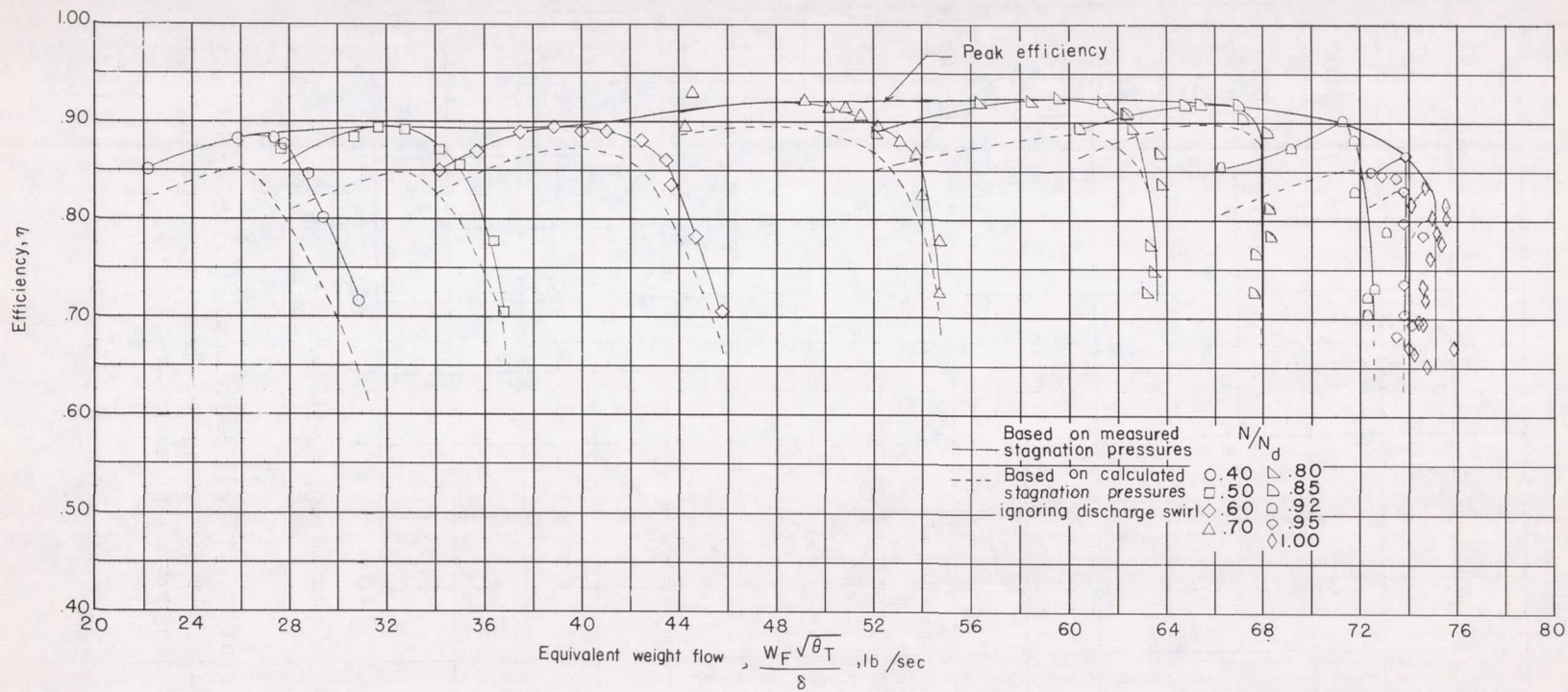


Figure 12.- Variation in compressor efficiency with rotational speed and weight flow.

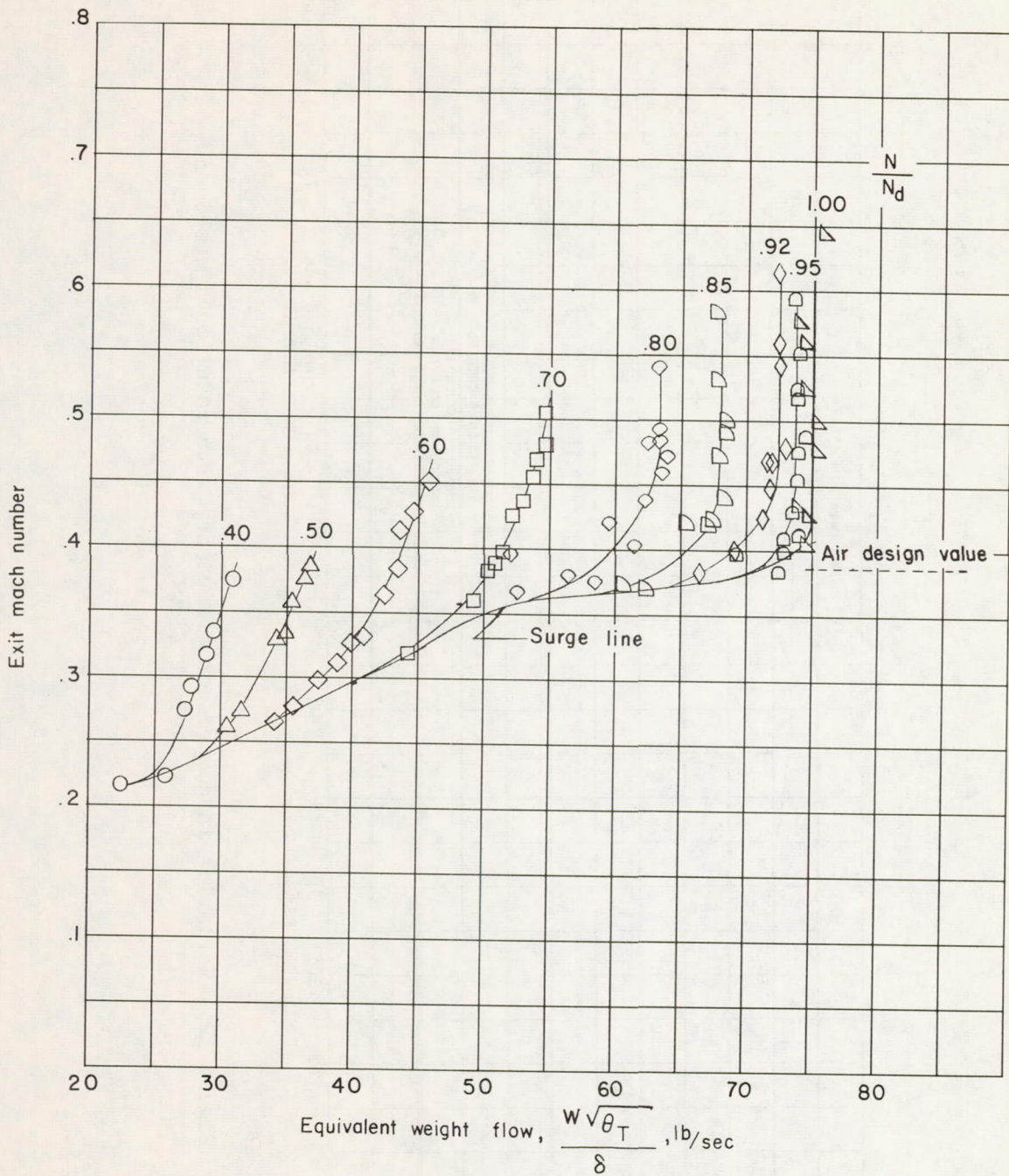


Figure 13.- Variation of exit Mach number with speed and weight flow. Discharge Mach numbers computed from outer casing static pressures and average stagnation pressures.

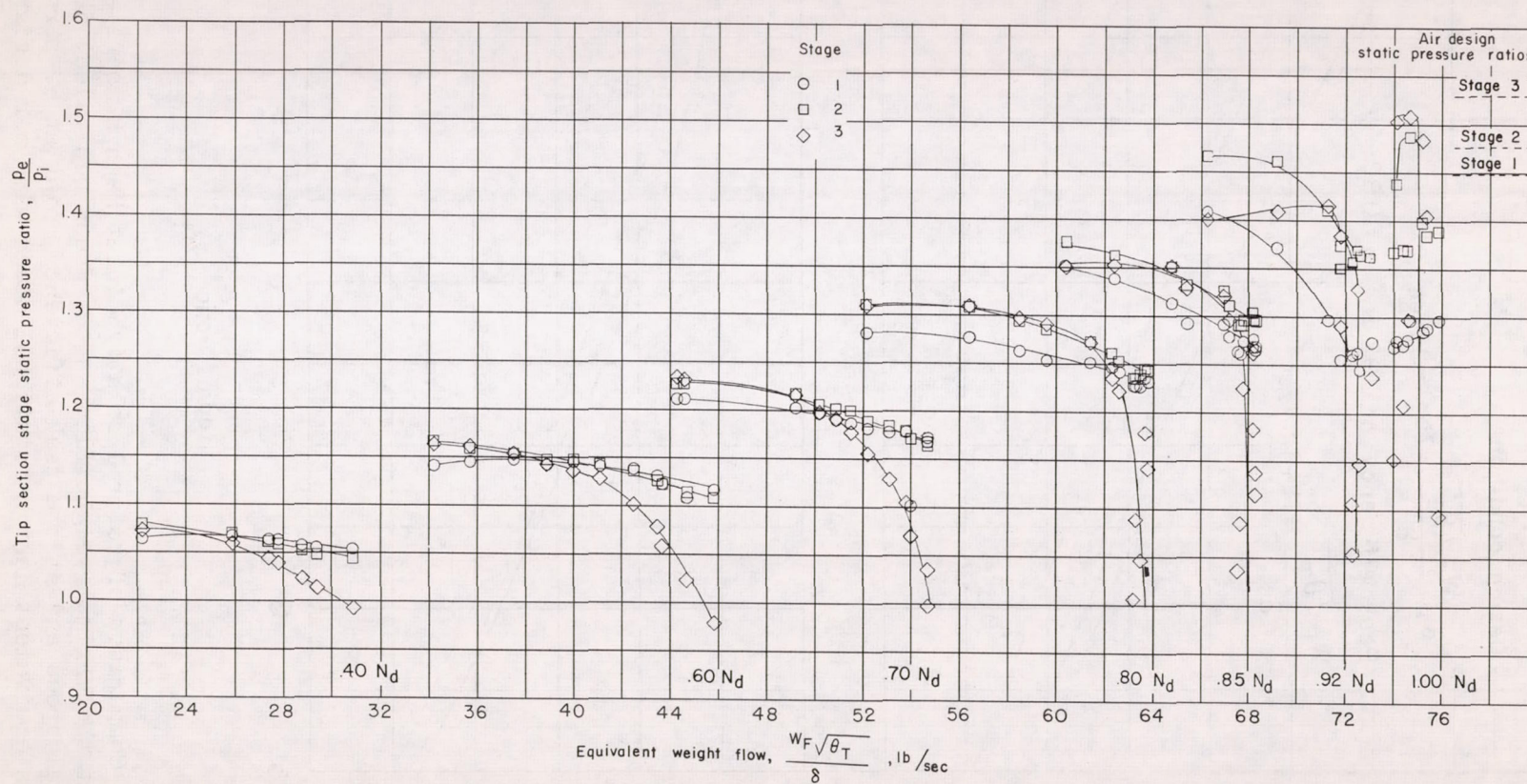


Figure 14.- Variation in stage tip section static pressure ratio with rotational speed and weight flow.

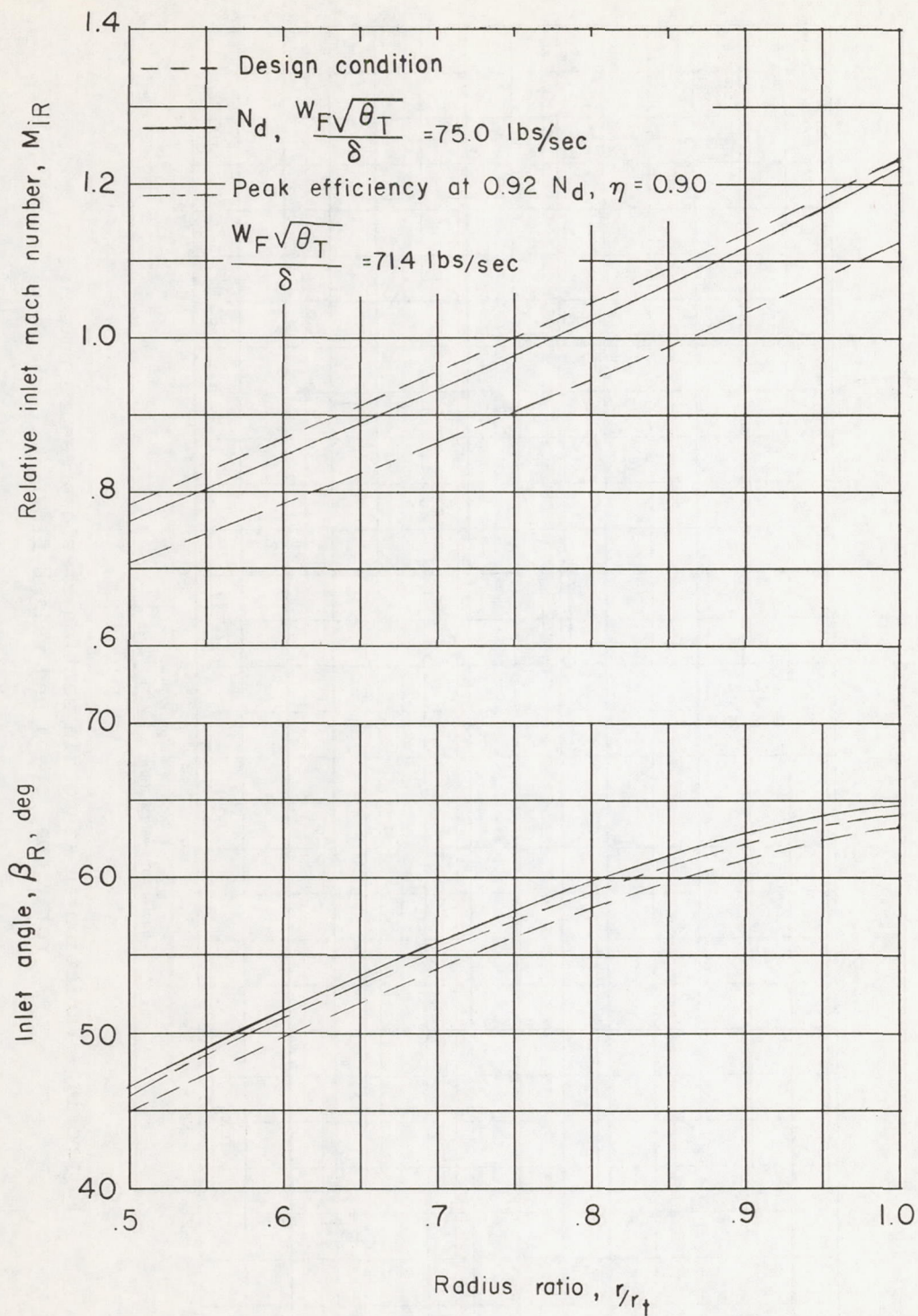


Figure 15.- Comparison of rotor 1 relative inlet Mach numbers and inlet angles at the maximum weight flow at the Freon equivalent design rotational speed and at the peak efficiency point at 92 percent of the Freon equivalent design rotational speed with air design values.

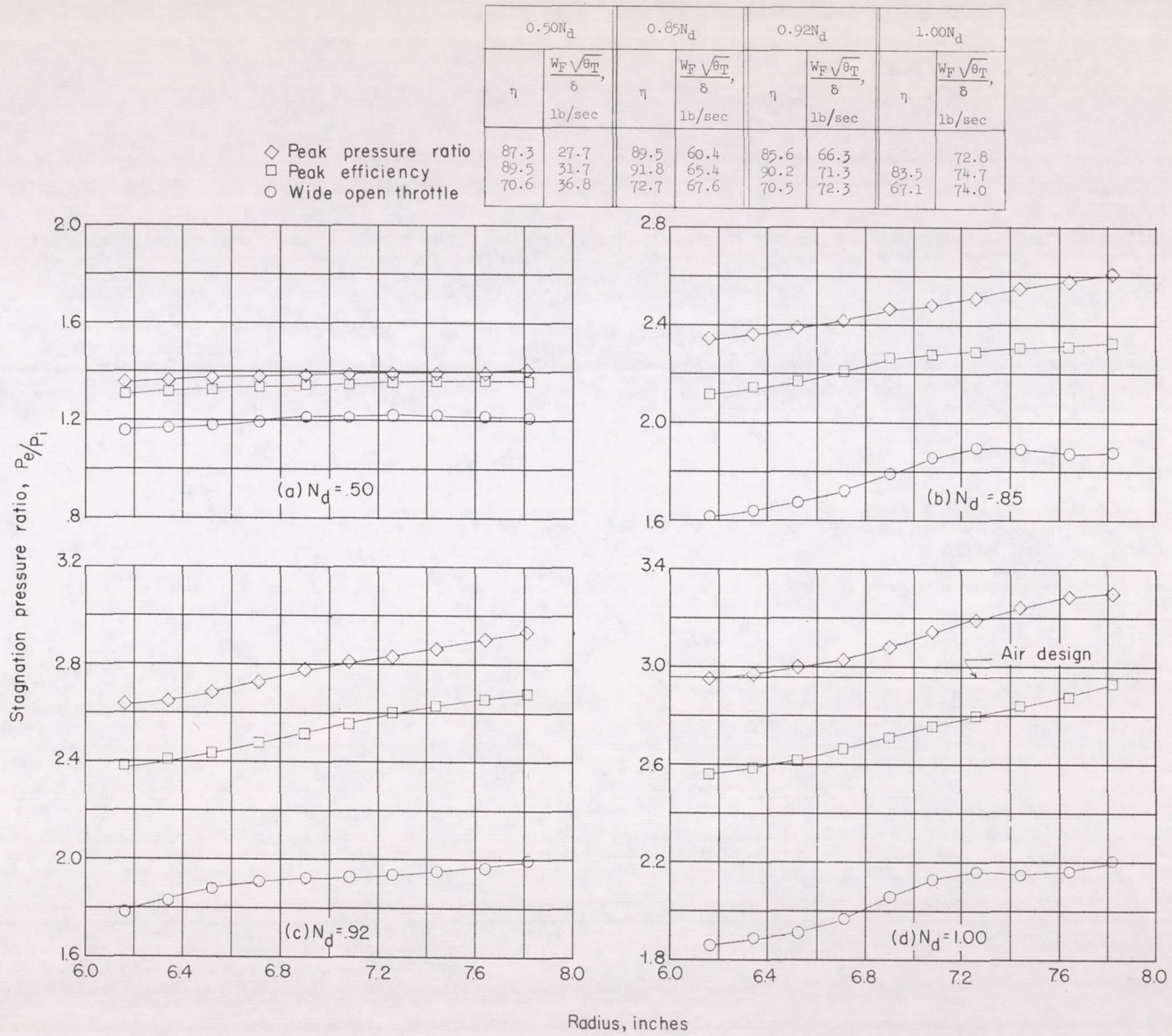


Figure 16.- Radial variation in overall stagnation pressure ratio at wide-open throttle, peak efficiency, and peak pressure ratio for several rotational speeds.